

Axisymmetric oscillations of magnetic neutron stars

Umin Lee^{1*}

¹*Astronomical Institute, Tohoku University, Sendai, Miyagi 980-8578, Japan*

Typeset 19 September 2018; Received / Accepted

ABSTRACT

We calculate axisymmetric oscillations of rotating neutron stars composed of the surface fluid ocean, solid crust, and fluid core, taking account of a dipole magnetic field as strong as $B_S \sim 10^{15}$ G at the surface. The adiabatic oscillation equations for the solid crust threaded by a dipole magnetic field are derived in Newtonian dynamics, on the assumption that the axis of rotation is aligned with the magnetic axis so that perturbations on the equilibrium can be represented by series expansions in terms of spherical harmonic functions $Y_l^m(\theta, \phi)$ with different degrees l for a given azimuthal wave number m around the the magnetic axis. Although the three component models can support a rich variety of oscillation modes, axisymmetric ($m = 0$) toroidal lt_n and spheroidal ls_n shear waves propagating in the solid crust are our main concerns, where l and n denote the harmonic degree and the radial order of the modes, respectively. In the absence of rotation, axisymmetric spheroidal and toroidal modes are completely decoupled, and we consider the effects of rotation on the oscillation modes only in the limit of slow rotation. We find that the oscillation frequencies of the fundamental toroidal torsional modes lt_n in the crust are hardly affected by the magnetic field as strong as $B_S \sim 10^{15}$ G at the surface. As the radial order n of the shear modes in the crust becomes higher, however, both spheroidal and toroidal modes become susceptible to the magnetic field and their frequencies in general get higher with increasing B_S . We also find that the surface g modes and the crust/ocean interfacial modes are suppressed by a strong magnetic field, and that there appear magnetic modes in the presence of a strong magnetic field.

Key words: stars : neutron – stars: oscillations – stars : rotation – stars : magnetic fields

1 INTRODUCTION

Recent discoveries of quasi-periodic oscillations (QPOs) in the giant flares of Soft Gamma-Ray Repeaters SGR 1806-20 (Israel et al 2005) and SGR 1900+14 (Strohmayer & Watts 2005) and the confirmation of the discoveries (Watts & Strohmayer 2006, Strohmayer & Watts 2006) have made promising asteroseismology for magnetars, neutron stars with an extremely strong magnetic field (see, e.g., Woods & Thompson 2004 for a review on SGRs). Israel et al (2005) discovered QPOs of frequencies ~ 18 , ~ 30 and ~ 90 Hz in the tail of the SGR 1806-20 hyperflare observed December 2004, and suggested that the 30 Hz and 90 Hz QPOs could be caused by seismic vibrations of the neutron star crust (see, e.g., Duncan 1998). Later on, in the hyperflare of SGR 1900+14, Strohmayer & Watts (2005) found QPOs of frequencies 28, 53.5, 84, and 155 Hz, and claimed that the QPOs could be identified as low l fundamental toroidal torsional modes in the solid crust of the neutron star. Although the interpretation in terms of the crustal torsional modes is promising, the mode identification cannot always be definite. In fact, if different classes of oscillation modes can generate similar periodicities and information other than the periods are not available for the QPOs, it is usually difficult to assign a class of oscillation modes to the periods observed in preference to other classes of modes. This is particularly true for high frequency QPOs (e.g., 625 Hz QPO, Watts & Strohmayer 2006; 1835 Hz QPO and less significant QPOs at 720 and 2384 Hz in SGR 1806-20, Strohmayer & Watts 2006), for which there exist various classes of modes that can generate the periodicities observed. In this case, the pattern of observed frequencies, that

* E-mail: lee@astr.tohoku.ac.jp

is, the observed frequency spectrum could be a key for mode identification and hence understanding the underlying neutron stars themselves. McDermott et al (1988) have carried out detailed modal analyses for neutron star models with a solid crust, but without the effects of magnetic field and rotation on the oscillation modes. Since the detected QPOs are thought to come from magnetors inferred to possess a strong magnetic field, it is useful to calculate oscillations of rotating neutron stars that have a solid crust and a strong magnetic field.

An extensive theoretical modal analysis of magnetic neutron stars having a solid crust was first carried out by Carroll et al (1986), who however employed a cylindrical geometry for the analysis of the neutron star models, and assumed a uniform magnetic field whose axis is parallel to the axis of the cylinder. The maximum strength of the magnetic field they examined is $B_S \sim 10^{12}$ G, which may be too weak for magnetors for which $B_S \gtrsim 10^{14}$ G is inferred. Carroll et al (1986) have suggested the existence of Alfvén modes and also found the transformation of the g modes in the surface ocean into magnetic modes as the field becomes stronger. More recently, Piro (2005) solved a simplified set of oscillation equations for toroidal torsional modes employing improved shear modulus (Strohmayer et al 1991) and up to date microphysics for equations of state to construct background neutron star models. Since the fluid core was ignored in the calculations by Carroll et al (1986) and Piro (2005), no reliable modal analyses were possible for spheroidal modes that can have substantial amplitudes in the core. In this paper, we calculate various oscillation modes of neutron star models that have a solid crust and are threaded by a dipole magnetic field. Since a non-radial mode of a spherical neutron star thereaded by a dipole magnetic field cannot be represented by a single spherical harmonic function, we employ series expansions to represent the perturbations accompanied by a mode. In §2, we give a brief description of method of solution we employ, numerical results are given in §3, and §4 is for conclusions. The oscillation equations are given in Appendix as well as boundary and jump conditions used in this paper.

2 METHOD OF SOLUTION

2.1 Perturbation Equations

To derive oscillation equations for a magnetized and rotating neutron star with a solid crust, we follow Carroll et al (1986), Lee & Strohmayer (1996), and Lee (2004). We consider no general relativistic effects on oscillations, that is, the oscillation equations are derived in Newtonian dynamics. We employ spherical polar coordinates (r, θ, ϕ) , whose origin is at the center of the star and the axis of rotation is the axis of $\theta = 0$. We assume a dipole magnetic field given by

$$\mathbf{B} = \mu_m \nabla (\cos \theta / r^2), \quad (1)$$

where μ_m is the magnetic dipole moment. For simplicity, we also assume that the magnetic axis coincides with the rotation axis. Since the dipole field is a force-free field such that $(\nabla \times \mathbf{B}) \times \mathbf{B} = 0$, the field does not influence the equilibrium structure of the star. Assuming the axis of rotation is also the magnetic axis, the temporal and angular dependence of perturbations can be given by a single factor $e^{i(m\phi + \omega t)}$, where m is the azimuthal wavenumber around the rotation axis and $\omega \equiv \sigma + m\Omega$ is the oscillation frequency observed in the corotating frame of the star where σ is the oscillations frequency in an inertial frame, and Ω is the angular frequency of rotation. The linearized basic equations applied in the solid crustal region of the star are then given by

$$-\omega^2 \boldsymbol{\xi} + 2i\omega \boldsymbol{\Omega} \times \boldsymbol{\xi} = \frac{1}{\rho} \nabla \cdot \boldsymbol{\sigma}' - \frac{\rho'}{\rho^2} \nabla \cdot \boldsymbol{\sigma} + \frac{1}{4\pi\rho} (\nabla \times \mathbf{B}') \times \mathbf{B} - \frac{1}{4\pi c} i\omega \mathbf{E}' \times \mathbf{B}, \quad (2)$$

$$\rho' + \nabla \cdot (\rho \boldsymbol{\xi}) = 0, \quad (3)$$

$$\frac{\rho'}{\rho} = \frac{1}{\Gamma_1} \frac{p'}{p} - \xi_r A, \quad (4)$$

$$\mathbf{B}' = \nabla \times (\boldsymbol{\xi} \times \mathbf{B}), \quad (5)$$

$$\mathbf{E}' = -i\omega \boldsymbol{\xi} \times \mathbf{B}/c, \quad (6)$$

where ρ is the mass density, p is the pressure, c is the velocity of light, $\boldsymbol{\xi}$ is the displacement vector, \mathbf{B}' and \mathbf{E}' are the Euler perturbations of magnetic and electric fields, respectively, and the other physical quantities with a prime (') denote their Euler perturbations, and A is the Schwarzschild discriminant defined by

$$A = \frac{d \ln \rho}{dr} - \frac{1}{\Gamma_1} \frac{d \ln p}{dr}, \quad (7)$$

and

$$\Gamma_1 = \left(\frac{\partial \ln p}{\partial \ln \rho} \right)_{ad}. \quad (8)$$

Note that we have employed the Cowling approximation neglecting the Eulerian perturbation of the gravitational potential, and that no effects of rotational deformation are included. In equation (2), σ' denotes the Euler perturbation of the stress tensor and is obtained from the Lagrangian perturbation defined in Cartesian coordinates by

$$\delta\sigma_{ij} = (\Gamma_1 pu)\delta_{ij} + 2\mu(u_{ij} - \frac{1}{3}u\delta_{ij}) \quad (9)$$

with u_{ij} being the strain tensor defined by

$$u_{ij} = \frac{1}{2} \left(\frac{\partial \xi_i}{\partial x_j} + \frac{\partial \xi_j}{\partial x_i} \right), \quad (10)$$

where δ_{ij} denotes Kronecker delta, μ is the shear modulus, and $u = \sum_{l=1}^3 u_{ll}$. The last term on the right-hand side of equation (2) represents the contribution from the displacement current, where infinite conductivity has been assumed. The linearized basic equations for a fluid region may be obtained by simply replacing the terms $\nabla \cdot \sigma$ and $\nabla \cdot \sigma'$ by $-\nabla p$ and $-\nabla p'$, respectively.

Since the angular dependence of perturbations on a rotating and magnetized star cannot be represented by a single spherical harmonic function, we expand the perturbed quantities in terms of spherical harmonic functions Y_l^m with different l s for a given m , on the assumption that the axis of rotation coincides with that of the magnetic field. The displacement vector ξ and the perturbed magnetic field \mathbf{B}' are then approximately represented by finite series expansions of length j_{\max} as

$$\frac{\xi}{r} = \sum_{j=1}^{j_{\max}} \left\{ [S_{l_j}(r) + H_{l_j}(r)\nabla] Y_{l_j}^m(\theta, \phi) + T_{l'_j}(r) \mathbf{e}_r \times \nabla Y_{l_j}^m(\theta, \phi) \right\} e^{i\omega t}, \quad (11)$$

and

$$\frac{\mathbf{B}'}{B_0(r)} = \sum_{j=1}^{j_{\max}} \left\{ [b_{l_j}^S(r) + b_{l'_j}^H(r)\nabla] Y_{l_j}^m(\theta, \phi) + b_{l_j}^T(r) \mathbf{e}_r \times \nabla Y_{l_j}^m(\theta, \phi) \right\} e^{i\omega t}, \quad (12)$$

and the pressure perturbation, p' , for example, is given by

$$p' = \sum_{j=1}^{j_{\max}} p_{l_j}'(r) Y_{l_j}^m(\theta, \phi) e^{i\omega t}. \quad (13)$$

where $B_0(r) = \mu_m/r^3$, and $l_j = |m| + 2(j-1)$ and $l'_j = l_j + 1$ for even modes, and $l_j = |m| + 2j - 1$ and $l'_j = l_j - 1$ for odd modes, respectively, and $j = 1, 2, 3, \dots, j_{\max}$. In this paper, we have used $j_{\max} = 12$. Substituting the expansions (11)~(13) into the linearized basic equations (2)~(6), and making use of equations (9) and (10), we obtain a finite set of coupled linear ordinary differential equations for the expansion coefficients such as $S_{l_j}(r)$ and $b_{l_j}^S(r)$, which we call the oscillation equations solved in the solid crust. The oscillation equations to be solved in magnetic fluid regions can be derived in the same manner (e.g., Lee 2004). The sets of oscillation equations thus obtained for the solid and fluid regions are given in Appendix A for the case of axisymmetric modes with $m = 0$. The boundary conditions at the center and the surface of the star and the jump conditions imposed at the interfaces between fluid and crustal regions are discussed in Appendix B. It is important to note that in the case of $\Omega = 0$ the oscillation equations for axisymmetric modes with $m = 0$ are decoupled into those for spheroidal modes and toroidal modes, respectively, and that axisymmetric spheroidal and toroidal modes are coupled only through the effects of rotation. For non-axisymmetric modes with $m \neq 0$, however there occurs no decoupling between spheroidal modes and toroidal modes even for $\Omega = 0$.

2.2 Non-Magnetic Core

In a fluid region where the magnetic pressure $p_B \equiv B_0^2(r)/8\pi$ is much smaller than the gas pressure p , that is, where the Alfvén velocity $v_A = \sqrt{2p_B/\rho}$ is much smaller than the sound velocity $\sim \sqrt{p/\rho}$ or $r\omega$, the magnetic perturbations \mathbf{b}^H and $i\mathbf{b}^T$ suffer very rapid spatial oscillations except for extremely low frequency oscillations (e.g., Lee 2004, see also Biront et al 1982, Roberts & Soward 1983, Cambell & Papaloizou 1986). This rapid spatial oscillation happens in the fluid core for both spheroidal and toroidal modes. For axisymmetric toroidal modes, for example, the dimensionless wavenumber k_r in the radial direction may be given by

$$k_r \sim r\omega/v_A, \quad (14)$$

and the wavenumber can be very large in the magnetic fluid region immediately below the crust where $p_B/p \ll 1$ even for $B_S = B_0(R) \sim 10^{15}$ G at the surface. Since this kind of rapid spatial oscillations usually do not occur in the solid crust, there exists an abrupt change in the property of the magnetic eigenfunctions across the boundary between the solid crust and the fluid core. Numerically, this means that we need an extremely large number of mesh points to correctly calculate

very short magnetic perturbations in the fluid core, which is not feasible. Since the rapid spatial oscillations in the magnetic perturbations come from the fact that the magnetic pressure significantly weaker compared to the gas pressure in the fluid core, it is legitimate to assume that the fluid core is non-magnetic so that the oscillation equations for non-magnetic fluid stars (e.g., Lee & Saio 1990) could be used. Assuming non-magnetic core, we neglect a possible dissipation of the oscillation energy due to Joule heating in the core.

3 NUMERICAL RESULTS

In this paper we mainly discuss the case of $\Omega = 0$, in which axisymmetric ($m = 0$) toroidal and spheroidal modes are decoupled. We briefly discuss the effects of rotation on the axisymmetric modes, assuming slow rotation so that $|\Omega/\sqrt{GM/R^3}| \ll 1$, in which case toroidal and spheroidal modes are only weakly coupled.

3.1 Equilibrium Models

The neutron star models we use consist of the surface fluid ocean, the solid crust, and the fluid core and are the same as those employed by McDermott et al (1988) for modal calculations without rotation and magnetic fields. The models are obtained from the fully general relativistic evolutionary cooling calculations of neutron stars by Richardson et al (1980). The outer crust extends down to the neutron drip point at $\rho = 4.3 \times 10^{11} \text{ g cm}^{-3}$ and is assumed to consist of bare Fe nuclei embedded in a uniform, neutralizing, degenerate electron gas. The strength of the Coulomb interaction between ions is characterized by the dimensionless parameter Γ , the ratio of the Coulomb energy to the thermal energy $k_B T$ with k_B being Boltzmann constant. The matter of the outer crust is assumed to undergo a first order fluid/solid phase transition at $\Gamma = 155$, and there exists the fluid ocean above the crystallization boundary at $\Gamma = 155$. In addition to the thermodynamic contributions from the nuclear and electronic kinetic energies, the equation of state used in the outer crust includes contributions from photons, the Coulomb interactions between nuclei and electrons, and nuclear vibrations and rotations. The inner crust extends from the neutron drip point at $4.3 \times 10^{11} \text{ g cm}^{-3}$ to the base of the crust at $2.4 \times 10^{14} \text{ g cm}^{-3}$ and it is assumed to consist of nuclei with $Z \sim 40$, degenerate electrons, and degenerate, nonrelativistic neutrons, where the actual composition of the nuclei in the inner crust is taken from Negele & Vautherin (1973). For the inner crust, the zero temperature equation of state is that by Negele & Vautherin (1973), and the leading order thermal corrections for the nuclei, electrons, and free neutrons are also included. At densities greater than $2.4 \times 10^{14} \text{ g cm}^{-3}$, the lattice is assumed to dissolve, and the core of the neutron star is taken to consist of a mixture of free and highly degenerate neutrons, protons, and electrons. The equation of state in the fluid core is that by Baym, Bethe, & Pethick (1971), and are added the leading thermal corrections for the three species. The outer most fluid envelope models are from the calculations by Gudmundsson et al (1983), and are fitted to the evolutionary core models by Richardson et al (1980) at mass density $\rho \approx 10^{10} \text{ g cm}^{-3}$. The more details of the models for oscillation calculations can be found in McDermott, van Horn, & Hansen (1988).

The shear modulus μ of the solid lattice is that given by Pandharipande, Pines, & Smith (1976):

$$\mu = 0.3711 \frac{Z^2 e^2 n_N^{4/3}}{2^{1/3}}, \quad (15)$$

where n_N is the number density of the nuclei. An improved calculation for the shear modulus was given by Strohmayer et al (1991). This improved shear modulus was used by several authors to calculate crustal oscillations of neutron stars, for example, by Duncun (1998) and Piro (2005). In this paper, we did not attempt to use improved models for modal calculations since our main concerns are to investigate the modal properties of magnetic neutron stars and not to try a detailed comparison between theoretical predictions and observational results for the QPOs from the SGRs.

For mode calculations in this paper, we mainly use neutron star models named NS05T7 and NS13T8, and the mass and radius of the former are $M = 0.503M_\odot$ and $R = 9.839\text{km}$, respectively, and those of the latter are $M = 1.326M_\odot$ and $R = 7.853\text{km}$, respectively. Both of the models have a solid crust, and the thickness of the crust is $\Delta r/R \sim 0.24$ for NS05T7 and $\Delta r/R \sim 0.055$ for NS13T8. The thickness of the surface ocean, on the other hand, is $\Delta r/R \sim 3.8 \times 10^{-5}$ for NS05T7 and $\Delta r/R \sim 2.3 \times 10^{-3}$ for NS13T8, respectively. The details of the physical parameters of these models are given in McDermott et al (1988).

3.2 Toroidal Modes

In Figure 1, the normalized frequencies $\bar{\omega} \equiv \omega/\sqrt{GM/R^3}$ of the axisymmetric ($m = 0$) toroidal torsional modes νt_n are plotted versus B_S for the models NS05T7 (top panel) and NS13T8 (bottom panel), where $B_S \equiv \mu_m/R^3$ is the strength of the dipole magnetic field at the surface. The frequencies $\bar{\omega}$ are local ones and for convenience the redshifted frequencies defined by $\nu_\infty \equiv \omega(1 - 2GM/Rc^2)^{1/2}/2\pi$ are also displayed on the right axis of the panels. We find that the frequencies $\bar{\omega}$

of the fundamental toroidal modes are only weakly affected by the dipole magnetic field of strength as large as $B_S \sim 10^{15}$ G at the surface, which is consistent with the results by Piro (2005). Note that the frequencies of the fundamental modes $_{l'}t_0$ show a slight decrease with increasing B_S for low values of l' . The overtone torsional modes $_{l'}t_n$ having $n \geq 1$ become more susceptible to the magnetic field as the radial order n gets higher and the wavelengths in the radial direction become shorter so that several wavelengths of the modes are spanned by the strong magnetic region in the outer most envelope (or crust). We find as a general trend the frequency of the overtone modes increases with increasing B_S . Besides the magnetic effect just mentioned, there exists a different kind of magnetic effects closely related to the fact that the separation of variables using a single spherical harmonic function is not possible for the oscillations of stars with a dipole magnetic field. In this case we may consider crustal toroidal modes with different l' s but with the same parity are coupled in the presence of the magnetic field. Since the toroidal modes with a given radial order $n \geq 1$ are nearly degenerate in frequency for different values of l' , the coupling effect brings about interference between them, which becomes significant as the field strength increases. As discussed by McDermott et al (1988) for non-magnetized neutron stars, the frequencies of the fundamental toroidal modes with different l' s approximately scale as¹

$$\bar{\omega}_{l'} \approx \sqrt{l'(l'+1)/6} \bar{\omega}_{l'=2}, \quad (16)$$

which is also confirmed even in the presence of a strong magnetic field $B_S \sim 10^{15}$ G.

The eigenfunctions $iT_{l'}$ and ib_l^T of the axisymmetric fundamental $_{l'}t_0$ mode of the model NS05T7 are depicted in Figure 2 for $B_S = 10^{12}$ G in panels (a) and (b) and for $B_S = 10^{15}$ G in panels (c) and (d), where the solid and dashed lines stand for $l' = 2$ and 4 for $iT_{l'}$ and for $l = 1$ and 3 for ib_l^T , and the amplitude normalization is given by $iT_{l'=2} = 1$ at the surface of the star. Different from the case with no magnetic field, the toroidal components $iT_{l'}$ of the displacement vector is continuous at the crust/ocean interface (see Carroll et al 1986). However, since we have assumed the fluid core is non-magnetic, no toroidal components $iT_{l'}$ and ib_l^T exist in the core for $\Omega = 0$. Both for $B_S = 10^{12}$ G and $B_S = 10^{15}$ G, $iT_{l'=2}$ dominates $iT_{l'=4}$ in the inner crust where $p_B \ll p$. For $B_S = 10^{12}$ G, the eigenfunctions $iT_{l'}$ and ib_l^T are approximately constant as functions of r/R , but for $B_S = 10^{15}$ G they are influenced by the strong magnetic field in the outer crust where the magnetic pressure p_B dominates the gas pressure p .

Reflecting the difference in the thickness of the solid crust between the two neutron star models, the normalized frequency spectra of the toroidal torsional modes show substantial differences. For example, the fundamental $_{l'}t_0$ modes of the model NS13T8 have normalized frequencies $\bar{\omega}$ lower than those of the model NS05T7, while the overtones of the former have higher $\bar{\omega}$ than the latter. This property remains the same even in the presence of a strong magnetic field. For the periods of the torsional modes of non-magnetic neutron stars, McDermott et al (1988) gave extrapolation formulae, in which the local periods are proportional to the radius of the star for the fundamental modes and to the crust thickness for the overtone modes for a given spherical harmonic degree l' . The normalized frequencies $\bar{\omega}$ in the figure are consistent with what the extrapolation formulae predict.

On a closer look at the behavior of the low frequency torsional modes of the model NS13T8 in Figure 1, one may find that the torsional modes suffer mode crossings with magnetic modes, for which the oscillation frequency increases rapidly with increasing B_S and the oscillation energy is dominated by the magnetic perturbations. In fact, if we calculate the energies defined by

$$E_K(r) = \frac{1}{2} \int_0^r \omega^2 \rho |\boldsymbol{\xi}|^2 dV, \quad E_B(r) = \frac{1}{8\pi} \int_0^r |\boldsymbol{B}'|^2 dV, \quad (17)$$

we find that $E_B(R)$ is much larger than $E_K(R)$ for the magnetic modes. Note that $\nabla \cdot \boldsymbol{\xi} = 0$ for toroidal magnetic modes. For more detail, see below §3.3.

3.3 Spheroidal Modes

Figure 3 plots the oscillation frequencies $\bar{\omega}$ of the low radial order spheroidal shear modes $_{l=2}s_n$ and the core/crust interfacial modes $_{l}i_2$ for the models NS05T7 (top panel) and NS13T8 (bottom panel). For the model NS05T7, also plotted are magnetic modes, labeled m_k , that are found in the presence of a strong magnetic field. Note that in this paper, we use the symbols $_{l}i_1$ and $_{l}i_2$ to denote the crust/ocean and core/crust interfacial modes, respectively, where the amplitudes of the former are strongly localized in a narrow region around the crust/ocean interface and the amplitudes of the latter are largest at the core/crust interface. The oscillation frequencies $\bar{\omega}$ of the spheroidal shear modes increase with increasing B_S and this frequency increase becomes more rapid for higher radial order n modes. As in the case of toroidal torsional modes, for a given radial order n , the spheroidal shear modes $_{l}s_n$ with different degrees l are nearly degenerate in frequency, and mode couplings between the

¹ As pointed out by one of the referees, the frequency scaling formula given by equation (16) is correct only for $l' \gg 1$, and a much better scaling formula should be $\bar{\omega}_{l'} \approx \sqrt{(l'-1)(l'+2)/4} \bar{\omega}_{l'=2}$ as one can easily verify by solving the simple case of a uniform density, uniform shear modulus oscillating crust.

shear modes become significant for strong B_S . Figure 3 also shows that the frequency of the core/crust interfacial modes $_{1i2}$ is hardly modified by the magnetic field as strong as $B_S = 10^{15}$ G, except that the interfacial modes of the model NS05T7 experience avoided crossings with magnetic modes, whose oscillation frequencies rapidly increase with increasing B_S .

As in the case of the toroidal torsional modes, the normalized frequency spectra of the spheroidal modes of the two models appear differently, reflecting the difference in the thickness of the crust. The different appearance for the shear modes of the two models can be understood by using an approximation formula for the period, which is proportional to the crust thickness (e.g., McDermott et al 1988).

The eigenfunctions H_l and b_l^H of a $_{2s1}$ mode of the model NS05T7 are plotted in Figure 4 for $B_S = 10^{12}$ G in panels (a) and (b) and for $B_S = 10^{15}$ G in panels (c) and (d), where the amplitude normalization is given by $S_{l1}(R) = 1$ at the surface. Note that because of the jump conditions applied at the interfaces between the solid crust and the fluid zones (see Appendix B), the horizontal component of the displacement vector is continuous at the outer interface, but it is discontinuous at the inner interface, at which almost free slippery jump conditions are employed. For $B_S = 10^{12}$ G, the eigenfunctions b_l^H exhibit zigzag behavior in the outer crust reflecting that of Γ_1 , which is caused by discontinuous change of equilibrium composition with increasing ρ . For $B_S = 10^{12}$ G, the expansion coefficients H_{l1} and b_{l1}^H are dominant over others, but for $B_S = 10^{15}$ G the first few components of H_l and b_l^H are comparable to each other, and the eigenfunctions in the outer crust are significantly modified by the strong field compared with those for the case of $B_S = 10^{12}$ G. As shown by Figure 4, the amplitude of b_l^H for $B_S = 10^{12}$ G is much larger than that for $B_S = 10^{15}$ G for the same amplitude normalization $S_{l1}(R) = 1$. However, if we compare the quantities $E_K(r)$ and $E_B(r)$, we find $E_K(R)$ is much larger than $E_B(R)$ for $B_S = 10^{12}$ G, but $E_K(R)$ and $E_B(R)$ are comparable to each other for $B_S = 10^{15}$ G so that the magnetic perturbations is important to determine the modal properties of the shear modes in the presence of a strong magnetic field.

In Figure 5, the frequency $\bar{\omega}$ of the fundamental $_{2f}$ mode of the model NS05T7 is plotted versus B_S . The $_{2f}$ mode heavily suffers mode crossings with high radial order shear modes $_{1s_n}$ as B_S increases, and no pure $_{2f}$ mode could be identified in the presence of a strong magnetic field. This is also the case for high frequency p modes for a strongly magnetized star. Note that, even at $B_S \sim 10^{12}$ G, the fundamental mode $_{2f}$ with $\bar{\omega} = 1.8862$ is affected by the shear mode $_{2s_{n=10}}$ that has the frequency $\bar{\omega} = 1.8726$ at $B_S = 0$.

The frequency $\bar{\omega}$ of the g_1 mode in the fluid ocean and that of the core/ocean interfacial mode $_{1=2i1}$ are plotted versus B_S for the model NS05T7 in Figure 6. The frequencies begin to decrease rapidly to zero beyond $B_S \sim 10^5$ G, suggesting the strong magnetic field suppresses these modes. This suppression may come from the dominance of the magnetic force over the buoyant force in the fluid ocean at large B_S . We obtain almost the same suppression of the surface g modes and the crust/ocean interfacial modes for the model MS13T8, but they can survive much stronger magnetic field $B_S \sim 10^{10}$ G. This may be because the fluid ocean of the hotter model NS13T8 is much thicker and has a more developed radiative region, compared to the model NS05T7, giving much stronger buoyant force for the modes. It is interesting to note that the result for the g and $_{1i1}$ modes in the fluid ocean in this paper is different from that obtained by Carroll et al (1986), who suggested that the frequency of g_1 proportionally increases with increasing B_S to be a magnetically dominating mode, which they called g/m modes. The reason for the discrepancy is probably the difference in the geometry of the models and the magnetic field configuration between the two calculations.

3.4 Magnetic Modes

For both toroidal and spheroidal modes, we find oscillation modes that can be regarded as magnetic modes, for which the frequency $\bar{\omega}$ rapidly increases with increasing B_S , and the magnetic energy $E_B(R)$ is dominant over the kinetic one $E_K(R)$, although its appearance looks different depending on the model structure, particularly, on the crust thickness. It is also important to note that there seem to exist critical strengths of the magnetic field beyond which magnetic modes are allowed to exist. We find that the low frequency torsional modes of the model NS13T8 are often affected by mode crossing with the magnetic modes, but that those of the model NS05T7 rarely suffer from the mode crossings within the frequency and magnetic field strength ranges we investigated in this paper. In the same parameter ranges as those for the toroidal torsional modes, we find magnetic modes interacting with the core/crust interfacial modes $_{1i2}$ for the model NS05T7, but no examples of the mode crossings of this kind are found for the model NS13T8.

As an example of the mode crossings between the torsional modes and magnetic modes found for the model NS13T8, we plot, in Figure 7, $\bar{\omega}$ of the $_{2t0}$ (left panel) and $_{2t1}$ (right panel) modes versus $\log B_S$. The panels are magnifications of the corresponding parts from Figure 1, and clearly indicate mode interactions with magnetic modes as B_S increases. It is interesting to note that between $B_S = 10^{12}$ G and $\sim 10^{13}$ G, the $_{2t1}$ mode also interact with sequences of modes whose frequencies decrease as B_S increases. Figure 8 shows an example of the eigenfunctions of a toroidal magnetic mode having $\bar{\omega} = 0.01557$ at $B_S = 10^{14.48}$ G for NS13T8, where the amplitude normalization is given by $iT_{l'=2} = 1$ at the surface. For this mode, the expansion coefficients $iT_{l'=2}$ and $ib_{l=1}^T$ are dominant, and the magnetic perturbation ib_l^T shows almost discontinuous change at the crust/ocean interface, and has almost negligible amplitudes in the fluid ocean. Figure 9 is an example of the

Table 1. Coefficient C_2 for axisymmetric ($m = 0$) modes for the models NS05T7 and NS13T8

Mode	NS05T7			NS13T8		
	$\bar{\omega}_0$	Period (ms)	C_2	$\bar{\omega}_0$	Period (ms)	C_2
$2t_0$	0.04019	18.6	-6.75×10^{-2}	0.01897	17.4	-1.26×10^{-1}
$2t_1$	0.3286	2.29	2.76×10^1	0.4534	0.727	2.10×10^2
$3t_0$	0.06352	11.8	-6.20×10^{-2}	0.03000	11.0	-8.31×10^{-2}
$3t_1$	0.3318	2.26	1.31×10^1	0.4539	0.726	1.05×10^2
$4t_0$	0.08517	8.81	-9.83×10^{-2}	0.04024	8.19	-6.39×10^{-2}
$4t_1$	0.3361	2.23	6.74×10^0	0.4546	0.725	6.94×10^1
$2i_1$	0.008282	90.6	1.03×10^2	0.03326	9.91	2.56×10^1
$3i_1$	0.01171	64.1	7.95×10^1	0.04703	7.01	1.92×10^1
$2i_2$	0.1029	7.30	1.10×10^1	0.01862	17.7	1.51×10^0
$3i_2$	0.1400	5.36	8.33×10^0	0.02889	11.4	2.52×10^0
$2s_1$	0.3093	2.43	-2.10×10^1	0.4512	0.731	-1.92×10^2
$2s_2$	0.5556	1.35	-5.37×10^1	0.7704	0.428	-1.84×10^2
$3s_1$	0.2884	2.60	-2.10×10^1	0.4494	0.734	-1.03×10^2
$3s_2$	0.5518	1.36	-9.51×10^0	0.7684	0.429	-1.02×10^2
$2f$	1.886	0.398	3.11×10^{-1}	1.434	0.230	1.39×10^{-1}
$2p_1$	4.038	0.186	2.09×10^{-1}	3.967	0.0831	1.42×10^{-2}

eigenfunctions of a spheroidal magnetic mode of $\bar{\omega} = 0.07965$ at $Bs = 10^{14.45}$ G for the model NS05T7, where the amplitude normalization is given by $S_{l=0}(R) = 1$. For this magnetic mode the first components $H_{l=2}$ and $b_{l=1}^H$ of the series expansion are not necessarily dominant over other components associated with higher ls . Note that the relative thickness of the surface ocean of the model NS13T8 is much larger than that of NS05T7.

3.5 Effects of Slow Rotation

For slow rotation, we may approximate the oscillation frequency of axisymmetric ($m = 0$) modes as

$$\bar{\omega} \approx \bar{\omega}_0 + C_2 \bar{\Omega}^2, \quad (18)$$

where $\bar{\omega}_0$ denotes the oscillation frequency for the non-magnetic and non-rotating case. Note that the linear term in Ω is proportional to m and does not appear for axisymmetric modes, and that no effects of rotational deformation of the equilibrium structure on the oscillation are included in our calculation and hence the second order effects exclusively come from the Coriolis force, which is dominant for low frequency modes with $\bar{\omega} \lesssim 1$ (e.g., Lee 1993). We tabulate in Table 1 the coefficients C_2 for several toroidal and spheroidal modes including torsional t_n and shear s_n modes for the models NS05T7 and NS13T8. Note that we have used the labels i_1 and i_2 to denote respectively the crust/ocean and core/crust interfacial modes for both the models. For the model NS05T7, the frequency of the $2i_1$ mode for $B_S = 0$ is lower than that of the $2i_2$, but for the model NS13T8 the frequency of the $2i_1$ mode is higher than that of the $2i_2$ mode. From the table, we find that the second order response of the fundamental toroidal modes to rotation is negative and small, but that of the t_n is positive and rather large in the sense that the frequency correction $C_2 \bar{\Omega}^2$ can be comparable to $\bar{\omega}_0$ itself for $\bar{\Omega} \sim 0.1$. This is particularly the case for the toroidal modes of the model NS13T8. In the same sense, the response of the low radial order spheroidal shear modes s_n with low l to rotation can be substantial as well, particularly for the model NS13T8. The effects of slow rotation on axisymmetric f and p_1 modes, however, are not significant, the result of which is consistent with the calculation by Saio (1981) for a polytropic star with the index $N = 3$ and $\Gamma_1 = 5/3$, who have however taken into account the effects of rotational deformation.

4 CONCLUSIONS

We have calculated axisymmetric ($m = 0$) oscillation modes of neutron star models that have a solid crust and are threaded by a dipole magnetic field. We find that the frequencies of the fundamental toroidal torsional modes are not affected significantly by the magnetic field as strong as $B_S \sim 10^{15}$ G at the surface, and that high radial order torsional and shear modes are susceptible to a magnetic field even if the strength at the surface is much less than $B_S \sim 10^{15}$ G. Because both spheroidal shear and toroidal torsional modes are almost degenerate in oscillation frequency for a given radial order n , the high radial order modes with different ls for a given n are easily coupled in the presence of a strong magnetic field. Since the f modes (and p modes) are embedded in the sea of high radial order shear modes with various ls that are sensitive to the magnetic

field, the f modes suffer mode crossings with the shear modes as B_S varies, and their identity may become ambiguous in the presence of a strong magnetic field.

We find that the g modes in the fluid ocean and the crust/ocean interfacial modes are suppressed in a strong magnetic field, the result of which contradicts that obtained by Carroll et al (1986), who showed that the ocean g modes will survive to be a magnetic mode, labeled m/g_k in their paper, as the magnetic field becomes strong. The reason for the contradiction may be attributable to the difference in the geometry of the oscillating stars and of the magnetic field, that is, Carroll et al (1986) calculated oscillation modes of cylindrical stars threaded by a uniform magnetic field. The strength of the magnetic field necessary to completely suppress the ocean g modes and the crust/ocean interfacial modes depends on neutron star models, and if a neutron star has a hot buoyant radiative region in the ocean, the modes can survive a magnetic field of $B_S \sim 10^{10}$ G or stronger, although their frequency spectrum could be largely modified by the field.

As a model for burst oscillations observed in many low mass X-ray binary (LMXB) systems (e.g., Strohmayer et al 1997, Strohmayer & Bildsten 2004, van der Klis 2004), Heyl (2004) and Lee (2004) proposed that the oscillations are produced by low frequency buoyant r modes propagating in the surface fluid ocean of accreting neutron stars in the systems (see also Lee & Strohmayer 2005, Heyl 2005). Since no effects of magnetic field are properly taken into account in their analyses, it is needed to reexamine the r mode model for burst oscillations, whether the buoyant r modes can survive a strong magnetic field of the neutron stars and how their frequency spectrum is modified by the field.

We have also examined the effects of slow rotation on the axisymmetric oscillation modes, although no effects of rotational deformation are included. Since the first order effects of rotation do not appear for axisymmetric modes with $m = 0$, it is the second order effects of rotation that appear first and are due to the Coriolis force when no rotational deformation is considered. The second order effects can be important for torsional modes and shear modes with radial order $n \geq 1$ in the sense that the second order corrections to the frequency due to rotation can be comparable to the frequency itself for $\bar{\Omega} \sim 0.1$. But, for SGR 1806-20, for example, the rotation period is estimated to be 7.56s (e.g., Israel et al 2005), implying that the underlying object is a very slow rotator in the neutron star standard so that $\bar{\Omega} \ll 1$ and $C_2\bar{\Omega}^2$ should be negligible compared to $\bar{\omega}_0$. The first order correction due to the Coriolis force for non-axisymmetric modes can be found in Lee & Strohmayer (1996).

We find magnetic modes for a strong magnetic field. Here, magnetic modes are regarded as a oscillation mode that exists only in the presence of a strong magnetic field, and whose frequency rapidly increases with increasing B_S . We also note that the magnetic modes have their oscillation energy dominantly possessed by the magnetic perturbations. The modal properties of the magnetic modes found by Carroll et al (1986), labeled m/g_k and a_k , are not the same as the properties of the magnetic modes found in this paper. Note that although the magnetic modes computed by Carroll et al (1986) reside in the fluid ocean, the magnetic modes found in this paper have amplitudes both in the fluid ocean and in the solid crust, and a large fraction of the oscillation energy resides in the crust, as indicated by Figures 8 and 9. We note that a simple magnetohydrodynamical system can support Alfvén waves, as well as fast and slow magneto-acoustic waves in fluids (e.g., Sturrock 1994), and we may expect almost the same modal structure even for a magnetic solid, in which torsional waves propagate (e.g., Carroll et al 1986). At this moment, however, we have no clear classification scheme for the magnetic modes, which makes it difficult to obtain a good understanding of the modes. Further studies are definitely necessary for magnatic modes of neutron stars with a solid crust, since the magnetic modes could be important observationally for magnetor as an agent triggering instability for flares.

Because of the assumption of non-magnetic core employed in this paper (§2.2), we completely ignore the possible existence of magnetosonic modes in the core and the possible coupling between core magnetic modes and crustal shear modes, for example. This assumption would be a serious flaw when we are interested in core (or more global) magnetic modes themselves. In fact, the crustal magnetic modes found in the present paper could be flawed in the sense that the assumption of non-magnetic core excludes from the beginning the possible existence of more global magnetic modes extending form the core to the crust. For non-magnetic modes such as crustal shear modes, however, so long as the field strength is less than $\sim 10^{15}$ G at the surface so that the magnetic pressure is much smaller than the gas pressure (and/or the shear modulus) in the inner crust (see, e.g., Fig. 3 of Carroll et al (1986) or Fig. 1 of Piro (2005)), reflection of crustal shear waves at the bottom of the crust is effective to establish crustal shear modes well trapped in the crust, and the effects of the coupling with core magnetic modes would be minor, for example, on the frequency spectrum of the crustal shear modes. For the field strength much larger than 10^{15} G, the confinement of crustal shear mode amplitudes into the crust would be imperfect and global treatment properly including the core will be necessary. As suggested by one of the referees, a differentially rotating magnetor progenitor would produce a toroidal magnetic field, for which the complexities possibly caused by mechanical coupling between the crust and the core could be avoided. This case may be important and worth careful examination. Recent discussions on the crust-core coupling of magnetic modes, leading to more global magnetic modes of neutron stars, are found in Levin (2006), Glampedakis, Samuelsson, & Andersson (2006), and Sotani, Kokkotas, & Stergioulas (2006).

The assumption of non-magnetic core also leads to neglect of another possible role played by perturbed magnetic field in the core. Several authors (e.g., Biront et al 1982, Roberts & Soward 1983, Cambell & Papaloizou 1986) have discussed for magnetic normal stars that in a deep fluid region where the magnetic pressure is much smaller than the gas pressure, magnetic

perturbations become extremely short, decoupled from mechanical perturbations, which leads to a dissipation of the oscillation energy. In this paper, however, because of the numerical difficulty in properly treating the abrupt change of wave properties between the solid crust and the fluid core, we have employed a simplifying assumption that the fluid core is non-magnetic. Although the assumption of non-magnetic core would be reasonably justified since in the fluid core the magnetic pressure p_B is much smaller than the gas pressure p , appropriate estimations of the dissipative effects of extremely short magnetic perturbations in the fluid core are necessary to see whether the dissipation is significant enough to damp the excitation of the torsional oscillations. We have almost the same difficulty in treating the outer boundary conditions, for which we have assumed for simplicity no emission of electromagnetic waves from the surface even if we include the displacement current term. Although Carroll et al (1986) (see also McDermott et al 1988) suggested that the damping effects due to emission of electromagnetic waves from the surface are negligible except for magnetic modes, labeled m/g_k and a_k , fully consistent calculations including the damping effects are obviously necessary.

In the giant flare of SGR 1806-20 observed December 2004, there exist reports on detection of QPOs at 18, 30, and 92.5 Hz (Israel et al 2005), at 18, 92.5, and 626.5 Hz (Watts & Strohmayer 2006), and at ~ 90 , ~ 150 , 625, and 1835 Hz, and at ~ 720 and 2384 Hz but with less significances (Strohmayer & Watts 2006). In the giant flare of SGR 1900+14 observed in August 1998, Strohmayer & Watts (2005) have also found detection of QPOs at 53.5, 84, and 155.5 Hz, and at 28 Hz with lower significance. Identifying the QPOs of low frequencies $\nu_\infty \lesssim 100$ Hz with the fundamental toroidal torsional modes with various l s is rather secure (McDermott et al 1988, Duncan 1998, Piro 2005), but identification of the middle to high frequency QPOs is not straightforward. In fact, QPOs with frequencies ~ 100 to ~ 1000 Hz can be generated by high l' νt_0 modes, or overtone modes $\nu t_{n \geq 1}$ with low l' , or low l spheroidal shear modes $\nu s_{n \geq 1}$, or core/crust interfacial modes νs_2 , depending on neutron star models, and there exist no unique solution to identification if the frequency is the only available information. For much higher frequency QPOs like that at 2384 Hz, low l fundamental modes νf must be added to the list of candidates for the QPOs, although much more energy will be required to excite the modes to observable amplitudes than that for toroidal crustal modes.

In this paper, we have been only concerned with axisymmetric modes with $m = 0$. If we extend our calculation to non-axisymmetric modes with $m \neq 0$, mode coupling effects will be much more significant in a strong magnetic field because both toroidal torsional and spheroidal shear modes are nearly degenerate in frequency for a given radial order n , which makes numerical analysis difficult and tedious. However, together with employing neutron star models constructed with up to date equations of state and shear modulus, the extension to non-axisymmetric modes will be inevitable in order to make possible serious comparisons between theoretical predictions and observations.

APPENDIX A: OSCILLATION EQUATIONS FOR A MAGNETIZED STAR FOR AXISYMMETRIC MODES WITH $M = 0$

In this Appendix, we give the oscillation equations for axisymmetric ($m = 0$) modes separately for even modes and for odd modes. In the followings, for a given matrix $F = (F_{i,j})$, we employ the symbols $[F]$, $\{F\}$, and $\langle F \rangle$ to indicate the matrices defined as

$$[F] = (F_{i,j+1}), \quad \{F\} = (F_{i+1,j}), \quad \langle F \rangle = (F_{i+1,j+1}) \quad (A1)$$

for $i, j = 1, 2, 3, \dots$.

A1 Even Modes

For the solid crust, we employ the dependent variables defined as

$$\mathbf{z}_1 = (S_{l_j}(r)), \quad \mathbf{z}_2 = (H_{l_j}(r)), \quad \mathbf{z}_3 = (iT_{l'_j}(r)), \quad \mathbf{z}_4 = \alpha_2 \left(\frac{1}{r^2} \frac{d}{dr} (r^3 \mathbf{z}_1) - [\Lambda_0] \mathbf{z}_2 \right) + 2\alpha_1 \frac{d}{dr} (r \mathbf{z}_1) + \frac{2p_B}{p} C_0 \mathbf{b}^H, \quad (A2)$$

$$\mathbf{z}_5 = \alpha_1 \left(r \frac{d\mathbf{z}_2}{dr} + \{1\} \mathbf{z}_1 \right) - \frac{4p_B}{p} \{M_1\} \mathbf{b}^H, \quad \mathbf{z}_6 = \alpha_1 r \frac{d\mathbf{z}_3}{dr} - \frac{4p_B}{p} [M_0] i \mathbf{b}^T, \quad \mathbf{b}^H = (b_{l'_j}^H(r)), \quad \mathbf{b}^T = (b_{l'_j}^T(r)), \quad (A3)$$

where

$$l_j = 2(j-1), \quad \hat{l}_j = 2j, \quad l'_j = 1 + 2(j-1) \quad \text{for } j = 1, 2, 3, \dots, \quad (A4)$$

and the oscillation equations are given by

$$r \frac{d\mathbf{z}_1}{dr} = -\frac{3\Gamma_1}{\alpha_3} \mathbf{z}_1 + \frac{\alpha_2}{\alpha_3} [\Lambda_0] \mathbf{z}_2 + \frac{1}{\alpha_3} \mathbf{z}_4 - \frac{1}{\alpha_3} \frac{2p_B}{p} C_0 \mathbf{b}^H, \quad (A5)$$

$$[M_0] r \frac{d\mathbf{z}_2}{dr} = 2 \left(1 - \frac{\alpha_1}{\alpha_3} \right) K \mathbf{z}_1 + \left([M_0] - \frac{1}{2} \frac{\alpha_2}{\alpha_3} [C_1] \right) \mathbf{z}_2 - \frac{1}{2\alpha_3} K \mathbf{z}_4 + \left(\frac{1}{\alpha_3} \frac{p_B}{p} K C_0 - \frac{1}{2} \mathbf{1} \right) \mathbf{b}^H, \quad (A6)$$

$$\{\mathbf{M}_1\} r \frac{d\mathbf{z}_3}{dr} = \left(\{\mathbf{M}_1\} - \frac{1}{2} \{C_0\} \right) \mathbf{z}_3 - \frac{1}{2} i \mathbf{b}^T, \quad (\text{A7})$$

$$\begin{aligned} r \frac{d\mathbf{z}_4}{dr} = & \left((U - 4 - c_1 \bar{\omega}^2) V \mathbf{1} - \frac{2p_B}{p} C_0 (2Q_1 + C_1) \right) \mathbf{z}_1 + \left((V - 2\alpha_1) [\Lambda_0] - \frac{4p_B}{p} C_0 [Q_1 \Lambda_0 + C_1] \right) \mathbf{z}_2 + c_1 \bar{\omega}^2 \nu V C_0 \mathbf{z}_3 \\ & + V \mathbf{z}_4 + [\Lambda_0] \mathbf{z}_5 - 4\alpha_1 r \frac{d\mathbf{z}_1}{dr} + \frac{4p_B}{p} (Q_0 \Lambda_1 - C_0) \mathbf{b}^H + c_1 \bar{\omega}^2 V \left(\frac{v_A}{c} \right)^2 ((Q_0 Q_1 - \mathbf{1}) \mathbf{z}_1 + 2 [Q_0 C_1] \mathbf{z}_2), \end{aligned} \quad (\text{A8})$$

$$\begin{aligned} r \frac{d\mathbf{z}_5}{dr} = & \left(V \{\mathbf{1}\} + \frac{4p_B}{p} \{\mathbf{M}_1\} (2Q_1 + C_1) \right) \mathbf{z}_1 + \left(-c_1 \bar{\omega}^2 V \mathbf{1} - 2\alpha_1 \mathbf{1} + 2\alpha_1 \langle \Lambda_0 \rangle + \frac{8p_B}{p} \{\mathbf{M}_1\} [Q_1 \Lambda_0 + C_1] \right) \mathbf{z}_2 \\ & + c_1 \bar{\omega}^2 \nu V \{\mathbf{M}_1\} \mathbf{z}_3 - \{\mathbf{1}\} \mathbf{z}_4 + (V - 3) \mathbf{z}_5 + \{\mathbf{1}\} 2\alpha_1 r \frac{d\mathbf{z}_1}{dr} + \frac{4p_B}{p} \left(\{\mathbf{M}_1\} + \frac{1}{2} \{C_0\} \right) \mathbf{b}^H \\ & + c_1 \bar{\omega}^2 V \left(\frac{v_A}{c} \right)^2 \langle \Lambda_0 \rangle^{-1} (-2 (3Q_0 Q_1 - 1 + Q_0 C_1) \mathbf{z}_1 - [4Q_0 Q_1 \Lambda_0 + 8Q_0 C_1] \mathbf{z}_2), \end{aligned} \quad (\text{A9})$$

$$\begin{aligned} r \frac{d\mathbf{z}_6}{dr} = & -c_1 \bar{\omega}^2 \nu V K \mathbf{z}_1 + c_1 \bar{\omega}^2 \nu V [M_0] \mathbf{z}_2 + \left(-c_1 \bar{\omega}^2 V \mathbf{1} - 2\alpha_1 (\mathbf{1} - \frac{1}{2} \Lambda_1) \right) \mathbf{z}_3 + (V - 3) \mathbf{z}_6 + \frac{4p_B}{p} \left([M_0] + \frac{1}{2} [C_1] \right) i \mathbf{b}^T \\ & - c_1 \bar{\omega}^2 V \left(\frac{v_A}{c} \right)^2 \Lambda_1^{-1} (6Q_1 C_0 + 4Q_1 Q_0 \Lambda_1 - C_1 C_0) \mathbf{z}_3, \end{aligned} \quad (\text{A10})$$

where $\mathbf{1}$ denotes the unit matrix, and

$$\bar{\omega} = \omega / \sqrt{GM/R^3}, \quad \nu = 2\Omega/\omega, \quad (\text{A11})$$

and

$$c_1 = \frac{(r/R)^3}{M_r/M}, \quad V = -\frac{d \ln p}{d \ln r}, \quad U = \frac{d \ln M_r}{d \ln r}, \quad p_B = \frac{B_0^2(r)}{8\pi}, \quad v_A = \sqrt{\frac{B_0^2(r)}{4\pi\rho}} \quad (\text{A12})$$

and

$$\alpha_1 = \frac{\mu}{p}, \quad \alpha_2 = \Gamma_1 - \frac{2}{3} \alpha_1, \quad \alpha_3 = \Gamma_1 + \frac{4}{3} \alpha_1, \quad (\text{A13})$$

and M and R are the mass and radius of the star, and G is the gravitational constant. Note that the terms proportional to $(v_A/c)^2$ come from the displacement current.

For fluid regions the dependent variables we use are defined as

$$\mathbf{y}_1 = \mathbf{z}_1, \quad \mathbf{y}_2 = \left(\frac{p'_{l_j}(r)}{pV} \right), \quad \mathbf{y}_3 = \mathbf{z}_2, \quad \mathbf{y}_4 = \mathbf{z}_3, \quad \mathbf{y}_5 = \frac{4p_B}{pV} \mathbf{b}^H, \quad \mathbf{y}_6 = \frac{4p_B}{pV} i \mathbf{b}^T, \quad (\text{A14})$$

and the oscillation equations are given by

$$r \frac{d\mathbf{y}_1}{dr} = \left(\frac{V}{\Gamma_1} - 3 \right) \mathbf{y}_1 - \frac{V}{\Gamma_1} \mathbf{y}_2 + [\Lambda_0] \mathbf{y}_3, \quad (\text{A15})$$

$$\begin{aligned} r \frac{d\mathbf{y}_2}{dr} = & \left((c_1 \bar{\omega}^2 + rA) \mathbf{1} + \frac{2p_B}{pV} C_0 (2Q_1 + C_1) \right) \mathbf{y}_1 + (1 - rA - U) \mathbf{y}_2 + \frac{4p_B}{pV} C_0 [Q_1 \Lambda_0 + C_1] \mathbf{y}_3 - c_1 \bar{\omega}^2 \nu C_0 \mathbf{y}_4 \\ & + \frac{f}{2} C_0 \mathbf{y}_5 + \frac{C_0}{2} r \frac{d\mathbf{y}_5}{dr} - c_1 \bar{\omega}^2 \left(\frac{v_A}{c} \right)^2 ((Q_0 Q_1 - \mathbf{1}) \mathbf{y}_1 + 2 [Q_0 C_1] \mathbf{y}_3), \end{aligned} \quad (\text{A16})$$

$$[M_0] r \frac{d\mathbf{y}_3}{dr} = -\frac{1}{2} \left(\frac{V}{\Gamma_1} - 4 \right) K \mathbf{y}_1 + \frac{1}{2} \frac{V}{\Gamma_1} K \mathbf{y}_2 + \left([M_0] - \frac{1}{2} [C_1] \right) \mathbf{y}_3 - \frac{1}{2} \left(\frac{4p_B}{pV} \right)^{-1} \mathbf{y}_5, \quad (\text{A17})$$

$$\{\mathbf{M}_1\} r \frac{d\mathbf{y}_4}{dr} = \left(\{\mathbf{M}_1\} - \frac{1}{2} \{C_0\} \right) \mathbf{y}_4 - \frac{1}{2} \left(\frac{4p_B}{pV} \right)^{-1} \mathbf{y}_6, \quad (\text{A18})$$

$$\begin{aligned} \{\mathbf{M}_1\} r \frac{d\mathbf{y}_5}{dr} = & -\frac{4p_B}{pV} \{\mathbf{M}_1\} (2Q_1 + C_1) \mathbf{y}_1 - \{\mathbf{1}\} \mathbf{y}_2 + \left(c_1 \bar{\omega}^2 \mathbf{1} - \frac{8p_B}{pV} \{\mathbf{M}_1\} [Q_1 \Lambda_0 + C_1] \right) \mathbf{y}_3 - c_1 \bar{\omega}^2 \nu \{\mathbf{M}_1\} \mathbf{y}_4 \\ & - f \{\mathbf{M}_1\} \mathbf{y}_5 - c_1 \bar{\omega}^2 \left(\frac{v_A}{c} \right)^2 \langle \Lambda_0 \rangle^{-1} (-2 (3Q_0 Q_1 - 1 + Q_0 C_1) \mathbf{y}_1 - [4Q_0 Q_1 \Lambda_0 + 8Q_0 C_1] \mathbf{y}_3), \end{aligned} \quad (\text{A19})$$

$$\begin{aligned} [M_0] r \frac{d\mathbf{y}_6}{dr} = & c_1 \bar{\omega}^2 \nu K \mathbf{y}_1 - c_1 \bar{\omega}^2 \nu [M_0] \mathbf{y}_3 + c_1 \bar{\omega}^2 \mathbf{y}_4 - \left(f [M_0] + \frac{1}{2} [C_1] \right) \mathbf{y}_6 \\ & + c_1 \bar{\omega}^2 \left(\frac{v_A}{c} \right)^2 \Lambda_1^{-1} (6Q_1 C_0 + 4Q_1 Q_0 \Lambda_1 - C_1 C_0) \mathbf{y}_4, \end{aligned} \quad (\text{A20})$$

where

$$f = rA - \frac{V}{\Gamma_1} + U + 3. \quad (\text{A21})$$

The non-zero elements of the matrices C_0 , C_1 , K , M_0 , M_1 , Q_0 , Q_1 , Λ_0 , and Λ_1 that appear in the above equations are given by

$$(Q_0)_{i,i} = J_{l+1}^m, \quad (Q_0)_{i+1,i} = J_{l+2}^m, \quad (Q_1)_{i,i} = J_{l+1}^m, \quad (Q_1)_{i,i+1} = J_{l+2}^m, \quad (\text{A22})$$

$$(C_0)_{i,i} = -(l+2)J_{l+1}^m, \quad (C_0)_{i+1,i} = (l+1)J_{l+2}^m, \quad (C_1)_{i,i} = lJ_{l+1}^m, \quad (C_1)_{i,i+1} = -(l+3)J_{l+2}^m, \quad (\text{A23})$$

$$(K)_{i,i} = \frac{J_{l+1}^m}{l+1}, \quad (K)_{i,i+1} = -\frac{J_{l+2}^m}{l+2}, \quad (\text{A24})$$

$$(\Lambda_0)_{i,i} = l(l+1), \quad (\Lambda_1)_{i,i} = (l+1)(l+2), \quad (\text{A25})$$

$$(M_0)_{i,i} = \frac{l}{l+1}J_{l+1}^m, \quad (M_0)_{i,i+1} = \frac{l+3}{l+2}J_{l+2}^m, \quad (M_1)_{i,i} = \frac{l+2}{l+1}J_{l+1}^m, \quad (M_1)_{i+1,i} = \frac{l+1}{l+2}J_{l+2}^m, \quad (\text{A26})$$

where $l = |m| + 2i - 2$ for $i = 1, 2, 3, \dots$, and

$$J_l^m \equiv \left[\frac{(l+m)(l-m)}{(2l-1)(2l+1)} \right]^{1/2}. \quad (\text{A27})$$

A2 Odd Modes

For the crust, we use the dependent variables defined as

$$\mathbf{z}_1 = (S_{l_j}(r)), \quad \mathbf{z}_2 = (H_{l_j}(r)), \quad \mathbf{z}_3 = (iT_{l'_j}(r)), \quad \mathbf{z}_4 = \alpha_2 \left(\frac{1}{r^2} \frac{d}{dr} (r^3 \mathbf{z}_1) - \Lambda_0 \mathbf{z}_2 \right) + 2\alpha_1 \frac{d}{dr} (r \mathbf{z}_1) + \frac{2p_B}{p} [C_0] \mathbf{b}^H, \quad (\text{A28})$$

$$\mathbf{z}_5 = \alpha_1 \left(r \frac{d\mathbf{z}_2}{dr} + \mathbf{z}_1 \right) - \frac{4p_B}{p} [M_1] \mathbf{b}^H, \quad \mathbf{z}_6 = \alpha_1 r \frac{d\mathbf{z}_3}{dr} - \frac{4p_B}{p} \{M_0\} i\mathbf{b}^T, \quad \mathbf{b}^H = (b_{l'_j}^H(r)), \quad \mathbf{b}^T = (b_{l'_j}^T(r)), \quad (\text{A29})$$

where

$$l_j = 2(j-1) + 1, \quad l'_j = 2j, \quad l'_j = 2(j-1) \quad \text{for } j = 1, 2, 3, \dots \quad (\text{A30})$$

The oscillation equations are then

$$r \frac{d\mathbf{z}_1}{dr} = -\frac{3\Gamma_1}{\alpha_3} \mathbf{z}_1 + \frac{\alpha_2}{\alpha_3} \Lambda_0 \mathbf{z}_2 + \frac{1}{\alpha_3} \mathbf{z}_4 - \frac{1}{\alpha_3} \frac{2p_B}{p} [C_0] \mathbf{b}^H, \quad (\text{A31})$$

$$\{M_0\} r \frac{d\mathbf{z}_2}{dr} = 2 \left(1 - \frac{\alpha_1}{\alpha_3} \right) \{K\} \mathbf{z}_1 + \left(\{M_0\} - \frac{1}{2} \frac{\alpha_2}{\alpha_3} \{C_1\} \right) \mathbf{z}_2 - \frac{1}{2\alpha_3} \{K\} \mathbf{z}_4 + \left(\frac{1}{\alpha_3} \frac{p_B}{p} \{K\} [C_0] - \frac{1}{2} \mathbf{1} \right) \mathbf{b}^H, \quad (\text{A32})$$

$$[M_1] r \frac{d\mathbf{z}_3}{dr} = \left([M_1] - \frac{1}{2} [C_0] \right) \mathbf{z}_3 - \frac{1}{2} i\mathbf{b}^T, \quad (\text{A33})$$

$$\begin{aligned} r \frac{d\mathbf{z}_4}{dr} = & \left((U - 4 - c_1 \bar{\omega}^2) V \mathbf{1} - \frac{2p_B}{p} C_0 (2Q_1 + C_1) \right) \mathbf{z}_1 + \left((V - 2\alpha_1) \Lambda_0 - \frac{4p_B}{p} C_0 (Q_1 \Lambda_0 + C_1) \right) \mathbf{z}_2 + c_1 \bar{\omega}^2 \nu V [C_0] \mathbf{z}_3 \\ & + V \mathbf{z}_4 + \Lambda_0 \mathbf{z}_5 - 4\alpha_1 r \frac{d\mathbf{z}_1}{dr} + \frac{4p_B}{p} [Q_0 \Lambda_1 - C_0] \mathbf{b}^H + c_1 \bar{\omega}^2 V \left(\frac{v_A}{c} \right)^2 ((Q_0 Q_1 - \mathbf{1}) \mathbf{z}_1 + 2Q_0 C_1 \mathbf{z}_2), \end{aligned} \quad (\text{A34})$$

$$\begin{aligned} r \frac{d\mathbf{z}_5}{dr} = & \left(V \mathbf{1} + \frac{4p_B}{p} M_1 (2Q_1 + C_1) \right) \mathbf{z}_1 + \left(-c_1 \bar{\omega}^2 V \mathbf{1} - 2\alpha_1 (\mathbf{1} - \Lambda_0) + \frac{8p_B}{p} M_1 (Q_1 \Lambda_0 + C_1) \right) \mathbf{z}_2 \\ & + c_1 \bar{\omega}^2 \nu V [M_1] \mathbf{z}_3 - \mathbf{z}_4 + (V - 3) \mathbf{z}_5 + 2\alpha_1 r \frac{d\mathbf{z}_1}{dr} + \frac{4p_B}{p} \left([M_1] + \frac{1}{2} [C_0] \right) \mathbf{b}^H \\ & + c_1 \bar{\omega}^2 V \left(\frac{v_A}{c} \right)^2 \Lambda_0^{-1} (-2(3Q_0 Q_1 - 1 + Q_0 C_1) \mathbf{z}_1 - (4Q_0 Q_1 \Lambda_0 + 8Q_0 C_1) \mathbf{z}_2), \end{aligned} \quad (\text{A35})$$

$$\begin{aligned} r \frac{d\mathbf{z}_6}{dr} = & -c_1 \bar{\omega}^2 \nu V \{K\} \mathbf{z}_1 + c_1 \bar{\omega}^2 \nu V \{M_0\} \mathbf{z}_2 + (-c_1 \bar{\omega}^2 V \mathbf{1} - 2\alpha_1 \mathbf{1} + \alpha_1 \langle \Lambda_1 \rangle) \mathbf{z}_3 + (V - 3) \mathbf{z}_6 \\ & + \frac{4p_B}{p} \left(\{M_0\} + \frac{1}{2} \{C_1\} \right) i\mathbf{b}^T - c_1 \bar{\omega}^2 V \left(\frac{v_A}{c} \right)^2 \langle \Lambda_1 \rangle^{-1} [6Q_1 C_0 + 4Q_1 Q_0 \Lambda_1 - C_1 C_0] \mathbf{z}_3. \end{aligned} \quad (\text{A36})$$

For fluid regions the dependent variables we use are

$$\mathbf{y}_1 = \mathbf{z}_1, \quad \mathbf{y}_2 = \left(\frac{p'_{l_j}(r)}{pV} \right), \quad \mathbf{y}_3 = \mathbf{z}_2, \quad \mathbf{y}_4 = \mathbf{z}_3, \quad \mathbf{y}_5 = \frac{4p_B}{pV} \mathbf{b}^H, \quad \mathbf{y}_6 = \frac{4p_B}{pV} i \mathbf{b}^T, \quad (\text{A37})$$

and the oscillation equations are then given by

$$r \frac{d\mathbf{y}_1}{dr} = \left(\frac{V}{\Gamma_1} - 3 \right) \mathbf{y}_1 - \frac{V}{\Gamma_1} \mathbf{y}_2 + \Lambda_0 \mathbf{y}_3, \quad (\text{A38})$$

$$\begin{aligned} r \frac{d\mathbf{y}_2}{dr} = & \left((c_1 \bar{\omega}^2 + rA) \mathbf{1} + \frac{2p_B}{pV} C_0 (2Q_1 + C_1) \right) \mathbf{y}_1 + (1 - rA - U) \mathbf{y}_2 + \frac{4p_B}{pV} C_0 (Q_1 \Lambda_0 + C_1) \mathbf{y}_3 - c_1 \bar{\omega}^2 \nu [C_0] \mathbf{y}_4 \\ & + \frac{f}{2} [C_0] \mathbf{y}_5 + \frac{[C_0]}{2} r \frac{d\mathbf{y}_5}{dr} - c_1 \bar{\omega}^2 \left(\frac{v_A}{c} \right)^2 ((Q_0 Q_1 - \mathbf{1}) \mathbf{y}_1 + 2Q_0 C_1 \mathbf{y}_3), \end{aligned} \quad (\text{A39})$$

$$\{M_0\} r \frac{d\mathbf{y}_3}{dr} = -\frac{1}{2} \left(\frac{V}{\Gamma_1} - 4 \right) \{K\} \mathbf{y}_1 + \frac{1}{2} \frac{V}{\Gamma_1} \{K\} \mathbf{y}_2 + \left(\{M_0\} - \frac{1}{2} \{C_1\} \right) \mathbf{y}_3 - \frac{1}{2} \left(\frac{4p_B}{pV} \right)^{-1} \mathbf{y}_5, \quad (\text{A40})$$

$$[\mathbf{M}_1] r \frac{d\mathbf{y}_4}{dr} = \left([\mathbf{M}_1] - \frac{1}{2} [C_0] \right) \mathbf{y}_4 - \frac{1}{2} \left(\frac{4p_B}{pV} \right)^{-1} \mathbf{y}_6, \quad (\text{A41})$$

$$\begin{aligned} [\mathbf{M}_1] r \frac{d\mathbf{y}_5}{dr} = & -\frac{4p_B}{pV} \mathbf{M}_1 (2Q_1 + C_1) \mathbf{y}_1 - \mathbf{y}_2 + \left(c_1 \bar{\omega}^2 \mathbf{1} - \frac{8p_B}{pV} \mathbf{M}_1 (Q_1 \Lambda_0 + C_1) \right) \mathbf{y}_3 - c_1 \bar{\omega}^2 \nu [\mathbf{M}_1] \mathbf{y}_4 - f [\mathbf{M}_1] \mathbf{y}_5 \\ & - c_1 \bar{\omega}^2 \left(\frac{v_A}{c} \right)^2 \Lambda_0^{-1} (-2(3Q_0 Q_1 - 1 + Q_0 C_1) \mathbf{y}_1 - (4Q_0 Q_1 \Lambda_0 + 8Q_0 C_1) \mathbf{y}_3), \end{aligned} \quad (\text{A42})$$

$$\begin{aligned} \{M_0\} r \frac{d\mathbf{y}_6}{dr} = & c_1 \bar{\omega}^2 \nu \{K\} \mathbf{y}_1 - c_1 \bar{\omega}^2 \nu \{M_0\} \mathbf{y}_3 + c_1 \bar{\omega}^2 \mathbf{y}_4 - \left(f \{M_0\} + \frac{1}{2} \{C_1\} \right) \mathbf{y}_6 \\ & + c_1 \bar{\omega}^2 \left(\frac{v_A}{c} \right)^2 \langle \Lambda_1 \rangle^{-1} [6Q_1 C_0 + 4Q_1 Q_0 \Lambda_1 - C_1 C_0] \mathbf{y}_4. \end{aligned} \quad (\text{A43})$$

The non-zero elements of the matrices C_0 , C_1 , K , M_0 , \mathbf{M}_1 , Q_0 , Q_1 , Λ_0 , and Λ_1 are given by

$$(Q_0)_{i,i} = J_l^m, \quad (Q_0)_{i,i+1} = J_{l+1}^m, \quad (Q_1)_{i,i} = J_l^m, \quad (Q_1)_{i+1,i} = J_{l+1}^m, \quad (\text{A44})$$

$$(C_0)_{i,i} = (l-1) J_l^m, \quad (C_0)_{i,i+1} = -(l+2) J_{l+1}^m, \quad (C_1)_{i,i} = -(l+1) J_l^m, \quad (C_1)_{i,i+1} = (l) J_{l+1}^m, \quad (\text{A45})$$

$$(K)_{i,i} = -\frac{J_l^m}{l}, \quad (K)_{i,i+1} = \frac{J_{l+1}^m}{l+1}, \quad (\text{A46})$$

$$(\Lambda_0)_{i,i} = l(l+1), \quad (\Lambda_1)_{i,i} = (l-1)l, \quad (\text{A47})$$

$$(M_0)_{i,i} = \frac{l+1}{l} J_l^m, \quad (M_0)_{i+1,i} = \frac{l}{l+1} J_{l+1}^m, \quad (\mathbf{M}_1)_{i,i} = \frac{l-1}{l} J_l^m, \quad (\mathbf{M}_1)_{i+1,i} = \frac{l+2}{l+1} J_{l+1}^m, \quad (\text{A48})$$

where $l = |m| + 2i - 1$ for $i = 1, 2, 3, \dots$.

Note that for axisymmetric modes with $m = 0$, the components H_{l_1} and $b_{l_1}^T$ for even modes and iT_{l_1} and $b_{l_1}^H$ for odd modes are missing. As is evident from the equations given above, if $\Omega = 0$, the oscillation equations for axisymmetric modes are separated into those for spheroidal and toroidal modes, respectively. In this case, we can obtain spheroidal modes and toroidal modes separately, and mode couplings between these two are brought about as a result of the effects of rotation.

APPENDIX B: BOUNDARY CONDITIONS AND JUMP CONDITIONS

The surface boundary conditions we use are the same as those given in Lee (2005), and they are at the stellar surface

$$\delta p/p = 0, \quad \mathbf{b}^S + L^+ \mathbf{b}^H = 0, \quad (\text{B1})$$

and

$$i \mathbf{b}^T = 0, \quad (\text{B2})$$

where $(L^+)^{ij} = \delta_{ij}(l'_j + 1)$, δp is the Lagrangian perturbation of the pressure, and

$$\mathbf{b}^S \equiv (b_{l'_j}^S(r)) = -\Lambda_1 K \mathbf{z}_1 - 2\Lambda_1 M_0 \mathbf{z}_2 - 2m \mathbf{z}_3. \quad (\text{B3})$$

Assuming the central region is a non-magnetic fluid core, the central boundary conditions we impose are the regularity conditions for the variables $r \mathbf{y}_1$ and $r \mathbf{y}_2$ at the center (see, e.g., Lee & Saio 1986).

For the jump conditions at the interfaces between the solid crust and fluid regions, we assume that the dipole magnetic fields are continuous at the interfaces, and that there appears no singularity in \mathbf{B}' at the interfaces. Then, with the continuity of the radial component of the displacement vector given by

$$z_1 = y_1, \quad (B4)$$

the conditions

$$[(\boldsymbol{\xi} \times \mathbf{B}) \cdot \mathbf{e}_\theta]_-^+ = 0, \quad [(\boldsymbol{\xi} \times \mathbf{B}) \cdot \mathbf{e}_\phi]_-^+ = 0, \quad (B5)$$

lead to

$$z_2 = y_3, \quad (B6)$$

and

$$z_3 = y_4, \quad (B7)$$

where $[F]_-^+ \equiv \lim_{\epsilon \rightarrow 0} [F(r + \epsilon) - F(r - \epsilon)]$. Note that the conditions (B5) are obtained by integrating the right hand side of equation (5) along a closed, infinitesimally small, curve that crosses the interface. The conditions (B4), (B6), and (B7) guarantee the continuity of the radial component of \mathbf{B}' at the interfaces because of equation (B3). Finally, we require the continuity of the three components of traction given by

$$[\delta\tau_{rr}^B + \delta\tau_{rr}^S]_-^+ = 0, \quad (B8)$$

$$[\delta\tau_{r\theta}^B + \delta\tau_{r\theta}^S]_-^+ = 0, \quad (B9)$$

and

$$[\delta\tau_{r\phi}^B + \delta\tau_{r\phi}^S]_-^+ = 0, \quad (B10)$$

where $\delta\tau_{ij}^S$ and $\delta\tau_{ij}^B$ are the ij components of the perturbed traction associated with bulk modulus and magnetic field, respectively, and they are given by

$$\delta\tau_{rr}^S = \sum_l \left\{ \alpha_2 \left[\frac{1}{r^2} \frac{d}{dr} (r^3 S_l) - l(l+1) H_l \right] + 2\alpha_1 \frac{d}{dr} (r S_l) \right\} Y_l^m, \quad (B11)$$

$$\delta\tau_{r\theta}^S = \alpha_1 \sum_{l,l'} \left[\left(r \frac{dH_l}{dr} + S_l \right) \frac{\partial Y_l^m}{\partial \theta} + r \frac{dT_{l'}}{dr} \frac{1}{\sin \theta} \frac{\partial Y_{l'}^m}{\partial \phi} \right], \quad (B12)$$

$$\delta\tau_{r\phi}^S = \alpha_1 \sum_{l,l'} \left[\left(r \frac{dH_l}{dr} + S_l \right) \frac{1}{\sin \theta} \frac{\partial Y_l^m}{\partial \phi} + r \frac{dT_{l'}}{dr} \frac{\partial Y_{l'}^m}{\partial \theta} \right], \quad (B13)$$

$$\delta\tau_{rr}^B = \frac{1}{4\pi} (B_r \delta B_r - B_\theta \delta B_\theta), \quad (B14)$$

$$\delta\tau_{r\theta}^B = \frac{1}{4\pi} (B_\theta \delta B_r + B_r \delta B_\theta), \quad (B15)$$

and

$$\delta\tau_{r\phi}^B = \frac{1}{4\pi} B_r \delta B_\phi. \quad (B16)$$

Note that

$$[B_i \delta B_j]_-^+ = [B_i (B'_j + \boldsymbol{\xi} \cdot \nabla B_j)]_-^+ = [B_i B'_j]_-^+, \quad (B17)$$

since $[\boldsymbol{\xi}]_-^+ = 0$ and $[\mathbf{B}]_-^+ = 0$ at the interface.

In this paper, all the jump conditions discussed above are applied at the interface between the solid crust and the fluid ocean. However, since we have assumed the fluid core extending below the solid crust is non-magnetic, we cannot use all the jump conditions at the interface between the solid crust and the fluid core. Here, we apply the jump conditions (B4), (B8), (B9), and (B10). In the limit of non-magnetized stars, these jump conditions reduce to free slippery conditions employed by McDermott et al (1988), and Lee & Strohmayer (1996). Because of the jump conditions we use, the horizontal and toroidal components of the displacement vector and the perturbed magnetic field are not necessarily continuous at the interface.

REFERENCES

Baym G., Bethe H.A., Pethick C. 1971, Nucl. Physc., A175, 225
 Biront D., Goossens M., Cousens A., Mestel L., 1982, MNRAS, 201, 619
 Campbell C.G., Papaloizou J.C.B., 1986, MNRAS, 220, 577
 Carroll B.W., Zweibel E.G., Hansen C.J., McDermott P.N., Savedoff M.P., Thomas J.H., Van Horn H.M., 1986, ApJ, 305, 767
 Duncan R.C. 1998, ApJ, 498, L45

Gudmundsson E.H., Pethick C.J., Epstein R.I., 1983, *ApJ*, 272, 286
 Glampedakis, K., Samuelsson, L., Andersson, N., 2006, *astro-ph/0605461*
 Heyl J.S., 2004, *ApJ*, 600, 939
 Heyl J.S., 2005, *MNRAS*, 361, 504
 Israel G., et al., 2005, *ApJ*, 628, L53
 Lee U., 1993, *ApJ*, 405, 359
 Lee U., 2004, *ApJ*, 600, 914
 Lee U., Saio H., 1986, *MNRAS*, 221, 365
 Lee U., Saio H., 1990, *ApJ*, 360, 590
 Lee U., Strohmayer T.E., 1996, *A&A*, 311, 155
 Lee U., Strohmayer T.E., 2005, *MNRAS*, 361, 659
 Levin Y. 2006, *MNRAS*, 368, L35
 McDermott P.N., Van Horn H.M., Hansen C.J., 1988, *ApJ*, 325, 725
 Negele J. W., Vautherin D., 1973, *Nucl. Phys.*, A207, 298
 Pandharipande V.R., Pines D., Smith, R.A. 1976, *ApJ*, 208, 550
 Piro A.L., 2005, *ApJ*, 634, L153
 Richardson M.B., Van Horn H.M., Ratcliff K.F., Malone R.C., 1982, *ApJ*, 255, 624
 Roberts P.H., Soward A.M., 1983, *MNRAS*, 205, 1171
 Saio H., 1981, *ApJ*, 244, 299
 Sotani, H., Kokkotas, K.D., Stergioulas, N., 2006, *astro-ph/0608626*
 Strohmayer T.E., Ogata, S., Iyetomi, H., Ichimaru, S., Van Horn, H.M., 1991, *ApJ*, 275, 679
 Strohmayer T.E., & Bildsten L., 2004, in *Compact Stellar X-Ray Sources*, ed. W.H.G. Lewin & M. van der Klis (Cambridge: Cambridge Univ. Press)
 Strohmayer T.E., Jahoda K., Giles B.A., & Lee U. 1997, *ApJ*, 486, 355
 Strohmayer T.E., Watts A.L., 2005, *ApJ*, 632, L111
 Strohmayer T.E., Watts A.L., 2006, submitted
 Sturrock P.A., 1994, *Plasma Physics* (Cambridge: Cambridge Univ. Press)
 van der Kils, M., 2004, *astro-ph/0410551*
 Watts A.L., Strohmayer T.E., 2006, *ApJ*, 637, L117
 Woods P.M., Thompson, C., 2004, *astro-ph/0406133*

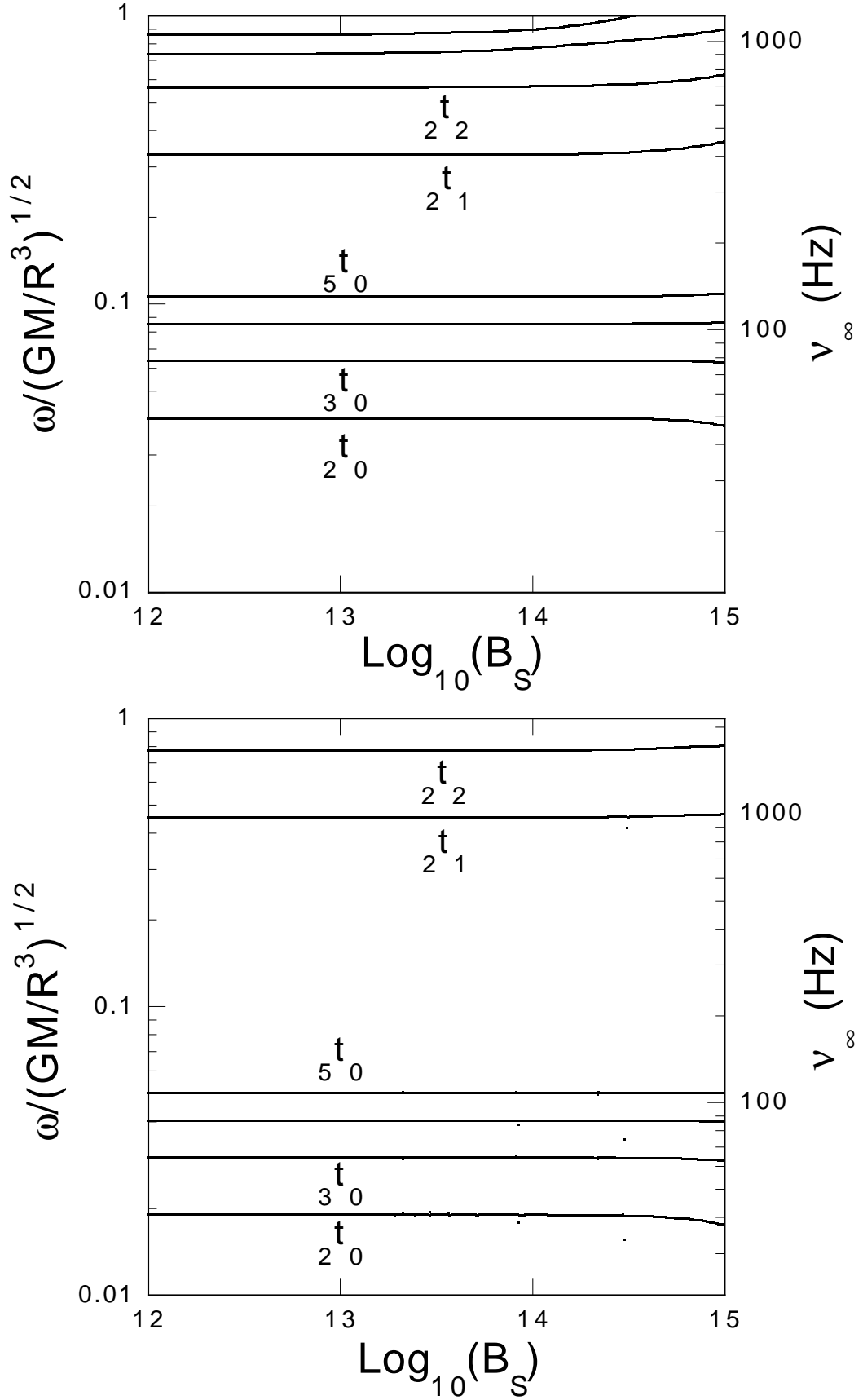


Figure 1. $\bar{\omega}$ versus $\log(B_S)$ for axisymmetric ($m = 0$) toroidal torsional modes νt_n of the neutron star models NS05T7 (top panel) and NS13T8 (bottom panel), where the fundamental torsional modes $\nu t_{n=0}$ for $l' = 2$ to 5, and the overtone modes $\nu = 2t_n$ for $n = 1$ to 4 for NT05T7 and for $n = 1$ and 2 for NS13T8 are shown. The frequency $\bar{\omega}$ shown is the local one, and $\nu_\infty = \omega (1 - 2GM/Rc^2)^{1/2} / 2\pi$ is the frequency at the surface of the star.

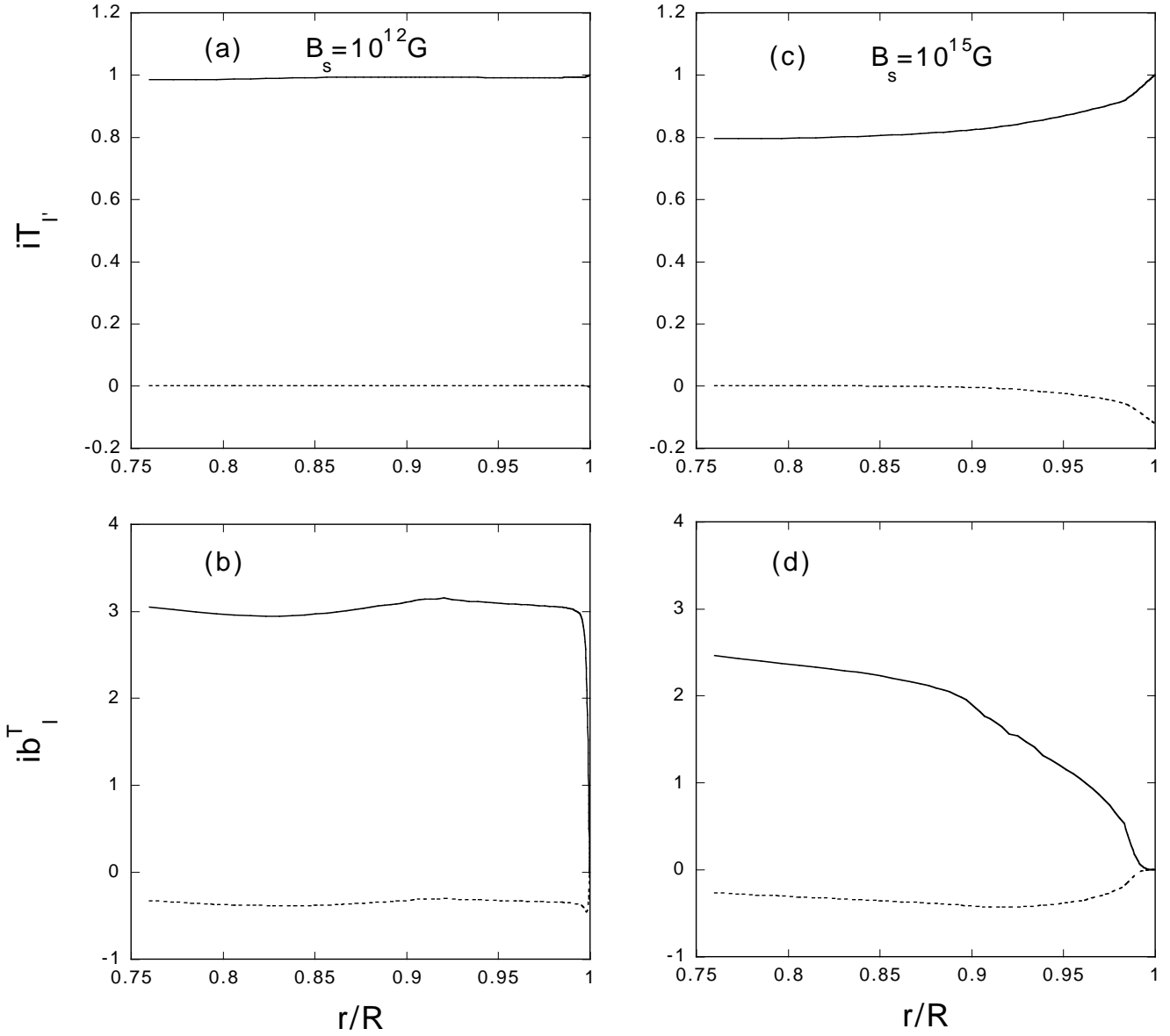


Figure 2. Eigenfunctions $iT_{l'}$ and ib_l^T of the axisymmetric ($m = 0$) fundamental toroidal torsional mode ${}_2t_0$ for $B_S = 10^{12}\text{G}$ in panels (a) and (b) and for $B_S = 10^{15}\text{G}$ in panels (c) and (d), where the solid lines stand for $iT_{l'=2}$ and $ib_{l=1}^T$, and the dashed lines for $iT_{l'=4}$ and $ib_{l=3}^T$, respectively. The amplitude normalization is given by $iT_{l'=2} = 1$ at the surface.

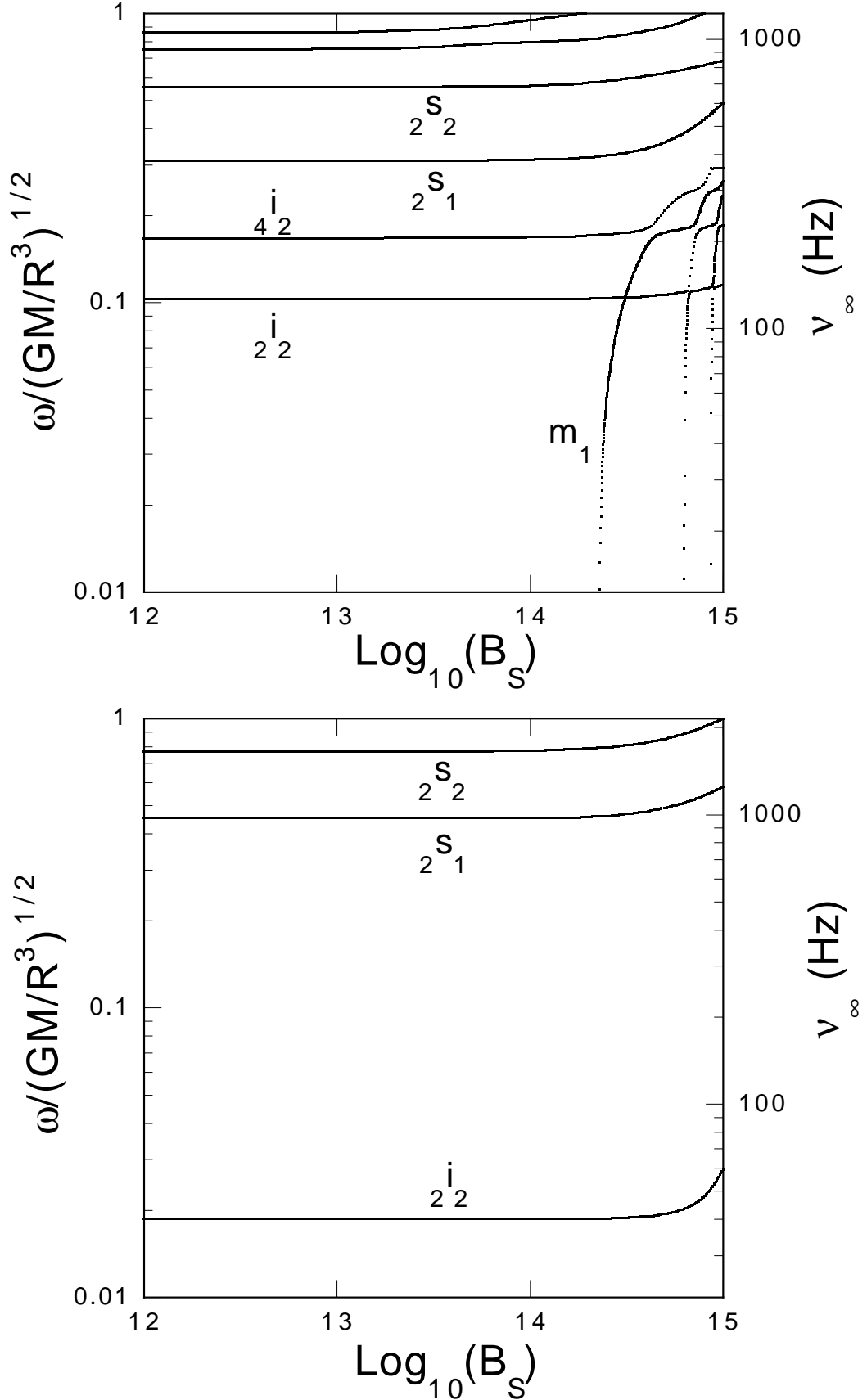


Figure 3. $\bar{\omega}$ versus $\log(B_S)$ for axisymmetric ($m = 0$) spheroidal shear modes ls_n and core/crust interfacial modes li_2 of the neutron star models NS05T7 (top panel) and NS13T8 (bottom panel), where the interfacial modes li_2 have large amplitudes at the interface between the solid crust and the fluid core. For the model NS05T7, magnetic modes, expediently labelled m_k , are also plotted. The frequency $\bar{\omega}$ shown is the local frequency $(1 - 8GM/R^3)^{1/2}/2$, which scales the right y-axis for each of the panels.

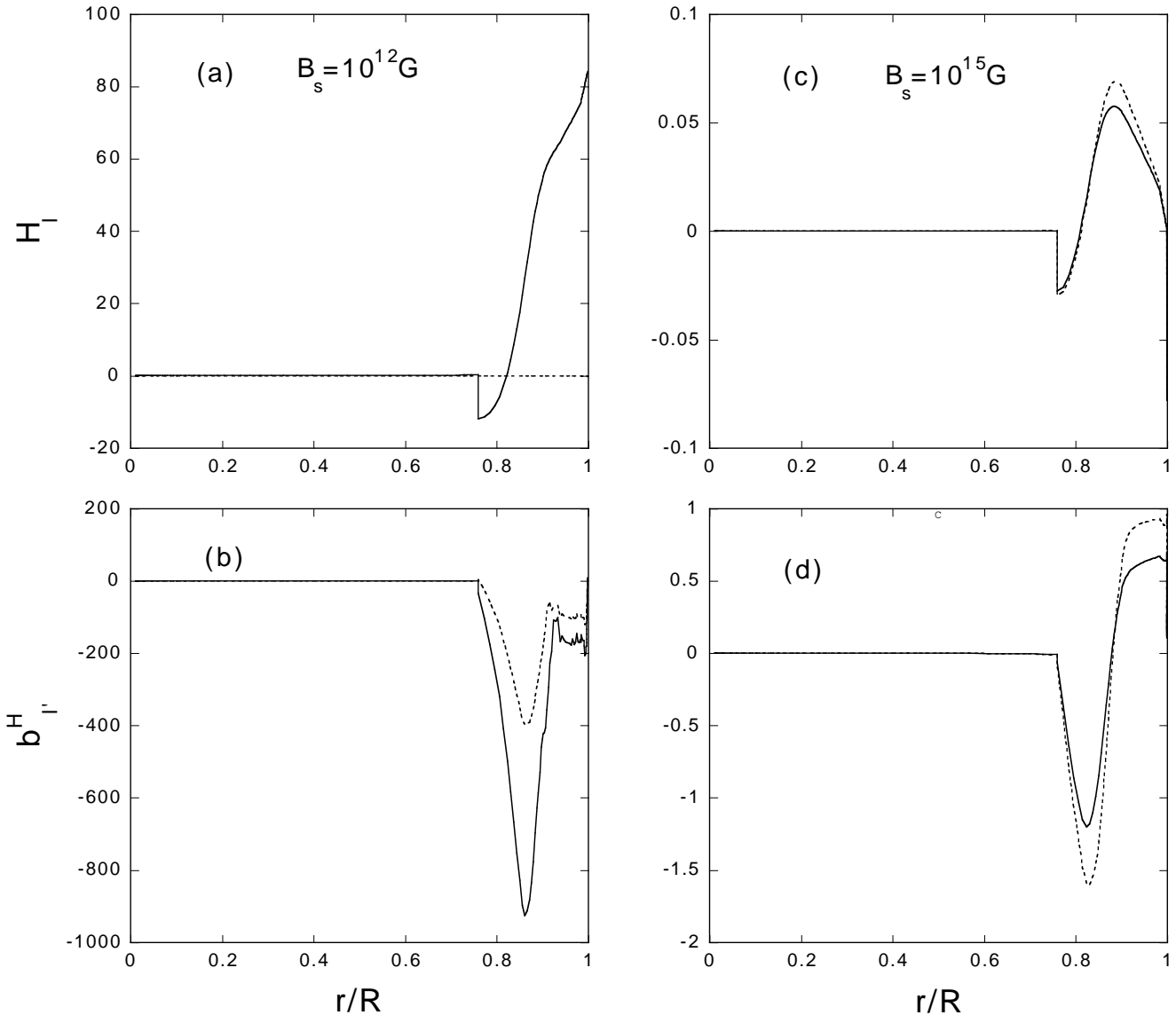


Figure 4. Eigenfunctions H_l and $b_{l'}^H$ of the axisymmetric ($m = 0$) spheroidal shear mode $2s_1$ for $B_s = 10^{12} \text{ G}$ in panels (a) and (b) and for $B_s = 10^{15} \text{ G}$ in panels (c) and (d), where the solid lines stand for $H_{l=2}$ and $b_{l'=1}^H$, and the dashed lines for $H_{l=4}$ and $b_{l'=3}^H$, respectively. The amplitude normalization is given by $S_{l=0} = 1$ at the surface.

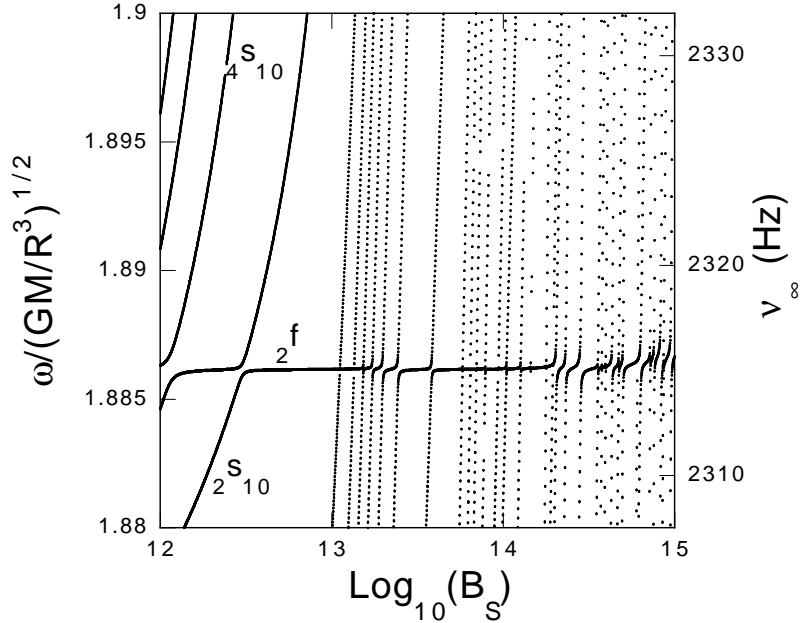


Figure 5. $\bar{\omega}$ versus $\log(B_S)$ for axisymmetric ($m = 0$) fundamental $l=2f$ mode of the neutron star model NS05T7. The $l=2f$ mode suffers mode crossings with high radial order shear modes ls_n as B_S increases. The frequency $\bar{\omega}$ shown is the local one, and $\nu_\infty = \omega (1 - 2GM/Rc^2)^{1/2} / 2\pi$ is also displayed on the right axis of the panel.

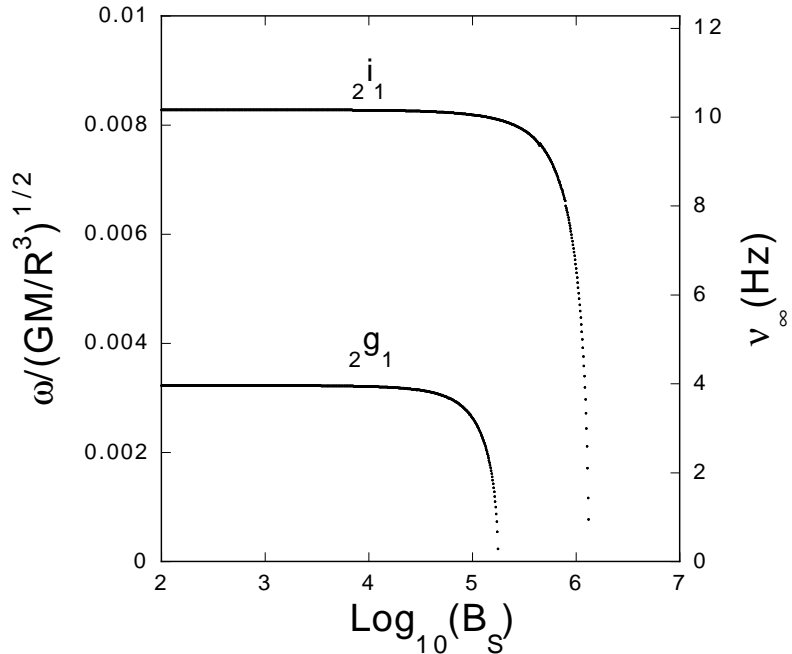


Figure 6. $\bar{\omega}$ versus $\log(B_s)$ for the axisymmetric ($m = 0$) $l=2g_{n=1}$ mode and the crust/ocean interfacial mode $l=2i_1$ whose amplitudes peak at the crust/ocean interface for the neutron star model NS05T7.

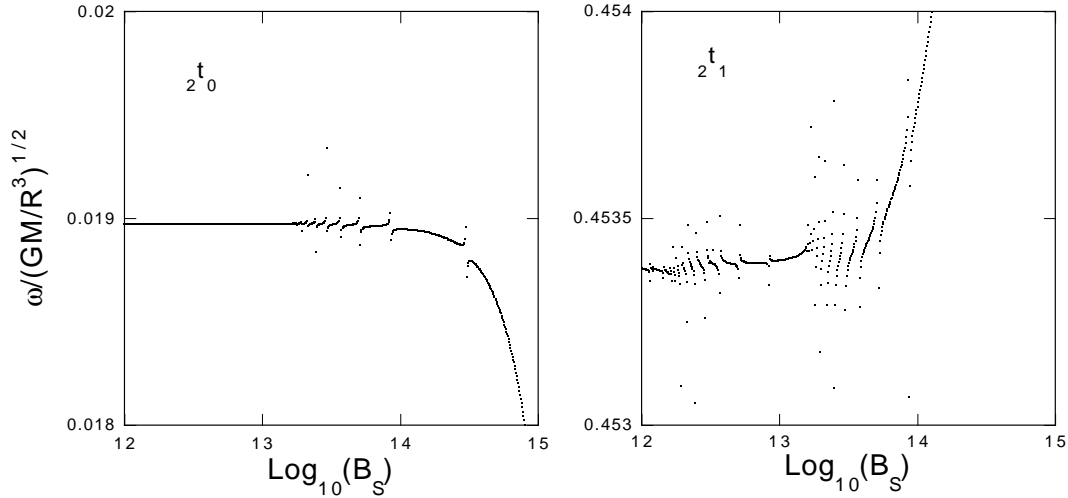


Figure 7. $\bar{\omega}$ versus $\log(B_s)$ for the fundamental torsional mode $2t_0$ (left panel) and the first overtone torsional mode $2t_1$ (right panel) of the model NS13T8. The panels are magnifications of the corresponding parts from Figure 1.

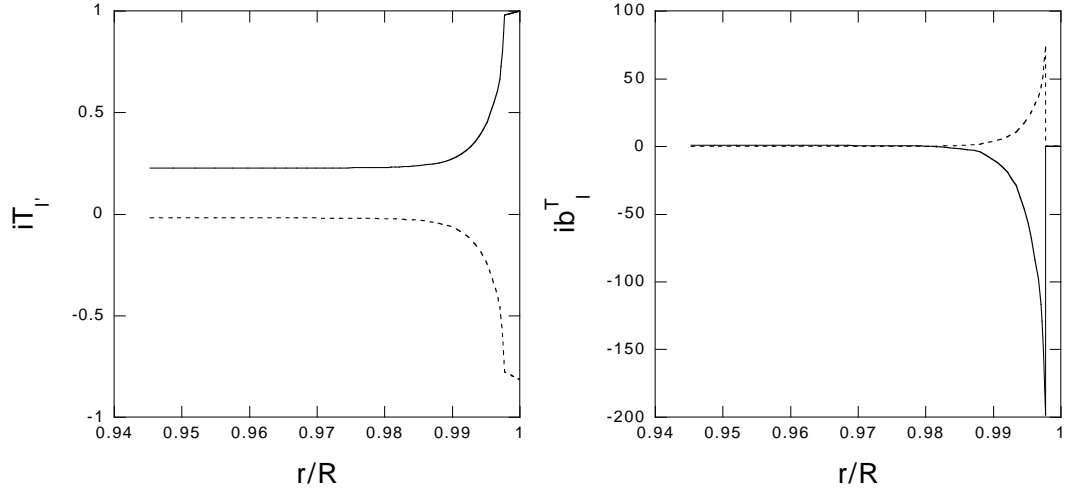


Figure 8. Eigenfunctions $iT_{l'}$ and ib_l^T of the $m = 0$ toroidal magnetic mode of $\bar{\omega} = 0.01557$ at $B_S = 10^{14.48}$ G for the model NS13T8, where the solid lines stand for $iT_{l'=2}$ and $ib_{l=1}^T$, and the dashed lines for $iT_{l'=4}$ and $ib_{l=3}^T$, respectively. The amplitude normalization is given by $iT_{l'=2} = 1$ at the surface.

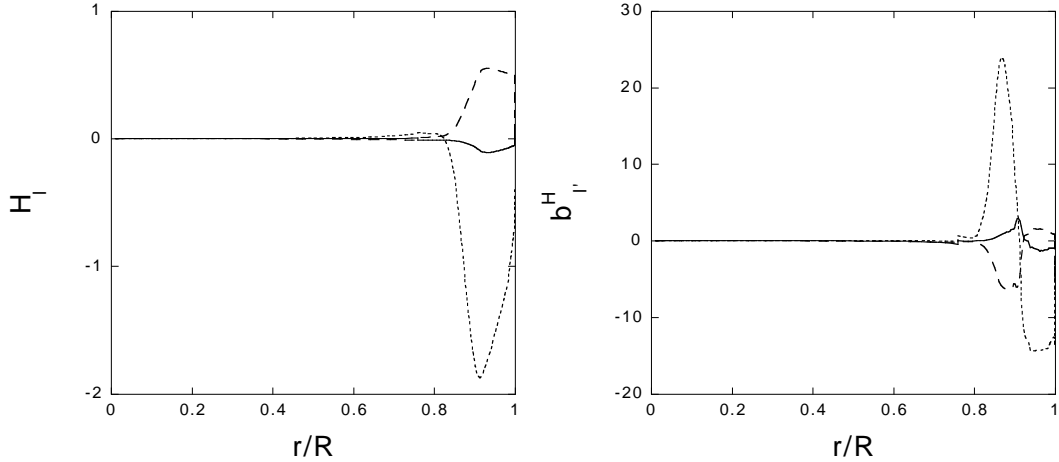


Figure 9. Eigenfunctions H_l and $b_{l'}^H$ of the $m = 0$ spheroidal magnetic mode labeled m_1 at $B_S = 10^{14.45}$ G for the model NS05T7, where the solid lines stand for $H_{l=2}$ and $b_{l'=1}^H$, the dashed lines for $H_{l=4}$ and $b_{l'=3}^H$, and the dotted lines for $H_{l=6}$ and $b_{l'=5}^H$, respectively. The amplitude normalization is given by $S_{l=0} = 1$ at the surface.